Optical Materials: X 2 (2019) 100017

Contents lists available at ScienceDirect

Optical Materials: X

journal homepage: www.journals.elsevier.com/optical-materials-x

Invited Article

Monolithic total internal reflection resonators for applications in photonics

Guoping Lin[a], Yanne K. Chembo[b,c,*]

[a] MOE Key Laboratory of Fundamental Physical Quantities Measurement, Hubei Key Laboratory of Gravitation and Quantum Physics, School of Physics, Huazhong University of Science and Technology, Wuhan, 430074, China

[b] University of Maryland, Department of Electrical and Computer Engineering, 8279 Paint Branch Dr, College Park, MD, 20742, USA

[c] Institute for Research in Electronics and Applied Physics (IREAP), 8279 Paint Branch Dr, College Park, MD, 20742, USA

ARTICLE INFO

Keywords:
Monolithic resonator
Whispering-gallery mode
Nonplanar ring oscillator
Total internal reflection
Second-harmonic
Third-harmonic
Optical parametric oscillation
Four-wave mixing
Stimulated Raman scattering
Stimulated brillouin scattering
Kerr combs

ABSTRACT

Monolithic total internal reflection resonators confine light through traveling-waves that can feature high quality factors and small mode volumes. Such resonators have emerged as rigid and compact platforms to explore high-efficiency laser-matter interactions and their related applications in photonics technology. In this review, we focus on monolithic ring resonators based on total internal reflection, with a particular emphasis on nonplanar ring oscillators and whispering-gallery mode lasers. We also discuss resonantly enhanced nonlinear photonic systems based on these resonators, using both non-centrosymmetric and centrosymmetric optical materials.

1. Introduction

Optical resonators have been key elements for the invention of the laser, where light fields can be spatially confined, spectrally filtered and temporally recirculated. A very common type of resonator is of the Fabry-Perot type, where light bounces back and forth from two highly reflecting mirrors facing each other, yielding a standing-wave pattern. In contrast, monolithic ring resonators (MRRs) are traveling-wave resonators, where the light travels in a low-loss bulk material in a closed path following an unambiguous direction of propagation [1]. These resonators can greatly reduce the mode volumes while preserving a large intracavity photon lifetime $\tau_{\rm ph}$, or equivalently, a high-quality factor $Q = \omega_0 \tau_{\rm ph}$, where ω_0 is the angular frequency of the photons. Therefore, owing to these enhanced photon lifetimes, strong light-matter interactions can be achieved in MRRs. This is why such resonators have become popular platforms to investigate fundamental phenomena and exploit a wide variety of optical materials for many practical applications.

MRRs in monolithic platforms have been developed in various configurations, as illustrated in Fig. 1. There are two main types of MRRs, categorized by the confinement methods.

In the first type, the waveguide resonators can be created using traditional on-chip waveguidess referred to as race-track resonators or using silica fiber rings, as shown in Fig. 1(a) [2–10]. Photonic bandgap structures can be used as well to confine light in a traveling-wave mode [11], as displayed in Fig. 1(b).

The second type of MRRs uses the principle of total internal reflection (TIR), and is the main focus of this review. Initially, monolithic TIR resonators were based only on very few surface reflections inside a glass or crystal resonator, as illustrated in Fig. 1(c). On the other hand, whispering-gallery mode resonators (WGMRs) [shown in Fig. 1(d)] can been seen as a MRRs based on hundreds or more TIRs instead of a few ones. WGM resonators have been at the center of a large body of literature since their inception in the early 20th century. In the last decades, applications based on WGM resonators have been explored in several fields such as optomechanics [12–14], optoelectronic oscillators [15–22], non-Hermitian photonics [23–25], sensors [26,27], nonlinear photonics [28–33], or gyroscopic sensing [34–37], just to name a few.

As indicated earlier, this review is focused on the monolithic ring resonators based on TIRs, as illustrated in Fig. 1(c and d). The outline of the article is the following. In Sec. 2, we first briefly introduce the basic principles of TIR MRRs. In particular, we present various types of WGM resonators, and discuss several topics such as coupling architectures used for WGM excitation, measurement methods for the high-Q resonances, WGM probing techniques, and thermal bistability. Section 3 is devoted to rare-earth-based lasers using nonplanar ring oscillators

* Corresponding author. University of Maryland, Department of Electrical and Computer Engineering, 8279 Paint Branch Dr, College Park, MD, 20742, USA.
E-mail address: ykchembo@umd.edu (Y.K. Chembo).

https://doi.org/10.1016/j.omx.2019.100017
Received 22 April 2019; Received in revised form 16 May 2019; Accepted 17 May 2019
Available online 27 June 2019

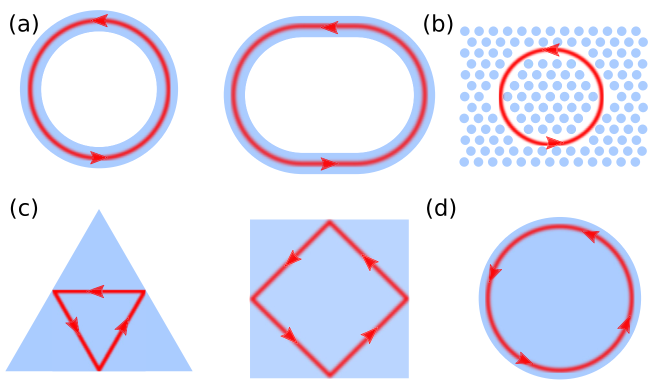

Fig. 1. Waveguide MRR: (a) Race-track resonator, (b) Photonic crystal ring resonator; Total internal reflection (TIR) MRR: (c) Traditional TIR resonator, (d) Whispering-gallery mode resonator. This review is focused on the monolithic ring resonators based on TIRs, corresponding to Fig. 1 (c,d).

(NPROs) and WGM resonators. The nonlinear photonic applications of traditional TIR MRRs and WGMRs covering second-order and third-order nonlinearity will be discussed ins Secs. 4 and 5, respectively. The last section will conclude the review.

2. Basics of traditional TIR MRRs and WGMRs

2.1. Traditional macroscopic TIR MRRs

Traditional macroscopic TIR ring resonators can be formed with a convenient setting of three or more mirrors [1]. For instance, four-mirror-based bow-tie resonators have been frequently used in solid-state laser systems. The fabrication of monolithic MRRs with bulk low-loss optical media is ideal to achieve a significant reduction for the size of the device as illustrated in Fig. 2. Light is usually confined within a single optical crystal through a few TIRs on side surfaces in one round-trip. In order to facilitate the coupling of light into cavity modes, one can choose to replace one TIR surface with high reflection coating as shown in Fig. 2 (a,b). Note that curved surfaces can be used as well for optical mode optimization when the thermal lensing effect is considered. Another way to couple light into and out of a TIR MRR is to use a prism coupler as illustrated in Fig. 2(c). For instance, fused silica TIR MRR with Q about 10^8 was reported in Ref. [38]. The applications of such macroscopic TIR MRRs in lasers and nonlinear frequency conversion will be discussed in the following sections.

2.2. Whispering-gallery mode cavities

In comparison to traditional TIR MRRs, light in a high-Q WGMR undergoes hundreds and up to tens of thousand TIRs in one round-trip within a circular cavity. Such resonators have been intensively investigated due to their capability of to feature ultra-high Q factors and small mode volumes. There have been several review articles introducing the fundamental principles and applications of WGM resonators, including for example refs. [26–33,39–52].

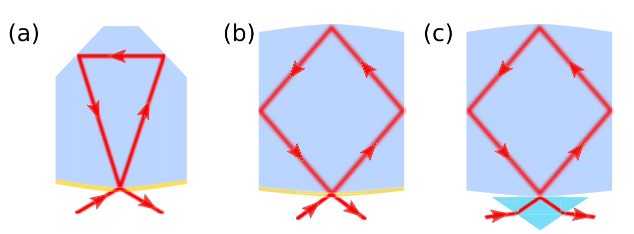

Fig. 2. The coupling methods for different types of TIR MRRs: (a,b) Free space coupling with one HR coated surface, (c) Evanescent wave coupling with an optical prism.

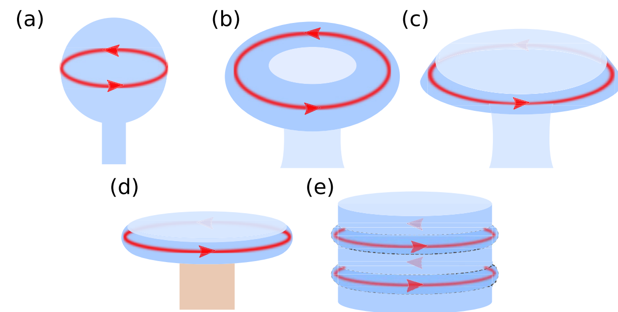

Fig. 3. The typical geometry of WGM resonators: (a) Sphere, (b) Toroid, (c) Wedge disk, (d) Disk with a curved edge, (e) Rings on a rod.

We focus here on discussing the development of WGM resonators from the standpoint of optical materials. Indeed, there have been many different types of WGM resonators including spheres, toroids, wedge-disks, curved rings on a disk and a rod, as illustrated in Fig. 3. In such WGM resonators, the free spectral range (FSR) of the resonant modes is usually calculated as $\Delta\nu_{\mathrm{FSR}} = c/2\pi nr$, where c is the speed of light in vacuum, n represents the effective index of refraction, r is the radius of the circular light path. This essential parameter typically ranges from few GHz to few THz depending on the size of the resonator.

2.2.1. Coupling methods for WGM resonators

As light is confined through TIRs in WGM resonators, the excitation of high-Q modes is generally not efficient when free-space coupling is used. Therefore, various efficient coupling approaches have been developed based on the evanescent wave coupling technique, and some of them are capable of exceeding a 90% efficiency. Fig. 4(a–c) illustrate the architectures representing WGM resonators coupled with a prism, a waveguide, an angle-tip waveguide [53–58]. In order to achieve high coupling efficiency, mode overlaps in both spectral and spatial domains should be taken into account. Moreover, the phase-matching condition requires that the speed of light in both the cavity and the coupler should be identical. As a result, the refractive index of the coupler is usually equal to or larger than that of the WGMR.

Bulk prism couplers can be used to excite high-Q modes in WGM resonators made from optical materials with very high refractive index. For instance, silicon prisms have been used to excite high-Q WGM resonators made from materials featuring high refractive indices such as diamond [59] and silicon itself [60]. On the other hand, optical waveguides such as tapered fibers or on-chip waveguides can also be fabricated or manufactured using various materials. Note that the phase-matched incident angle of TIR on the surface of a prim coupler is estimated by $\sin\theta_i = n_c/n_r$, where θ_i is the incident angle for the TIR on the surface of the coupler, while $n_{c,r}$ are the refractive indices of the coupler and the resonance mode, respectively. In the case of waveguide side-coupling, phase-matching requires that the refractive index of the waveguide mode matches the one of a resonance mode.

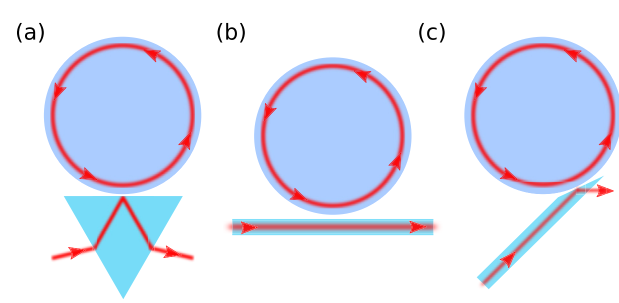

Fig. 4. The efficient coupling methods for WGM resonators: (a) Prism coupling, (b) Waveguide side-coupling, (c) Waveguide tip-coupling.

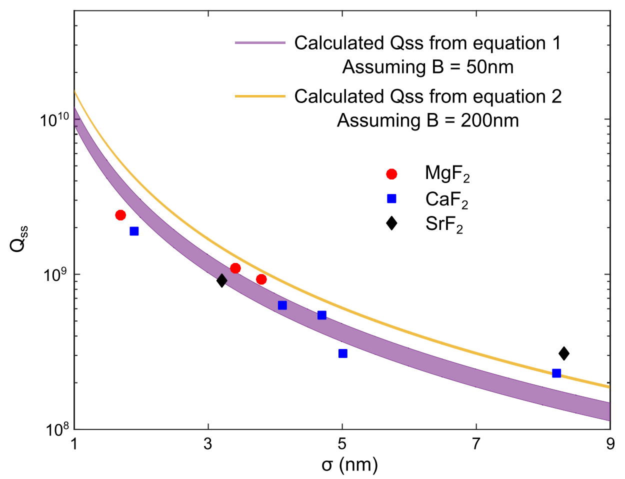

Fig. 5. The dependence of Q factors on the rms surface roughness, with a comparison between experimental results and theoretical expectations. Adapted with permission from Ref. [61], © 2018 Optical Society of America.

2.2.2. Surface roughness requirement

The main advantage of a WGMR is its capability to achieve ultra-high Q factors above 10^8 within a small volume [30,39]. The Q-factors depend on the optical transparency of the host material and the geometry profile of the resonator. The intrinsic Q_{int} factor of a WGMR is expressed as $Q_{\text{int}}^{-1} = Q_{\text{rad}}^{-1} + Q_{\text{abs}}^{-1} + Q_{\text{surf}}^{-1}$, where the sub-indices 'rad', 'abs' and 'surf' indicate the curvature-induced radiation loss, the absorption of intrinsic host material and the scattering loss from surface roughness, respectively.

In a WGM resonator with a radius larger than few tens of micrometers, the radiation loss term Q_{rad} is already greater than 10^{15}, and is usually disregarded for larger cavities. The absorption limited term Q_{abs} is calculated by $Q_{\text{abs}} = 2\pi n_r/(\lambda\alpha)$, where λ is the wavelength and α is the absorption coefficient. If we consider an α of 10^{-4} cm^{-1} for a material with $n_r = 1.5$ at $\lambda = 1.5$ µm, then the Q_{abs} value is as large as $\sim 10^{14}$, and does not appear as a limiting factor. Therefore, the intrinsic Q is mainly determined by the rms (root mean square) surface roughness when assuming an ideal curvature, and it is important to have the smoothest resonator surface in order to optimize the intrinsic quality factor.

Fig. 5 shows the experimental data on the Q-factors for mm-size WGM resonators as a function on the rms surface roughness [61]. Different fluoride materials including magnesium fluoride (MgF_2), calcium fluoride (CaF_2) and strontium fluoride (SrF_2) were mechanically polished into disk-shaped WGM resonators. The rms roughness values were measured using a white light Mirau-type interferometric microscope. Two theoretical models are used to match the experimental data when different correlation lengths are used [54,62]. One can see that a rms roughness smaller than 3 nm is required to achieve Q-factors larger than 10^9, and more details about this analysis can be found in Ref. [61]. To date, various WGM resonators made with glass and crystalline host materials have reached Q factors in the order 10^9 in different spectral ranges [63–71]. The largest Q factor is in the order of 10^{11}, and it was reported in Ref. [67] using a CaF_2 WGMR.

2.2.3. Measurement methods for high-Q WGMs

The high Q-factors corresponding to low-loss resonators can be measured using different methods. The simplest one is to sweep the resonance frequency with a probe laser and measure the full linewidth at half maximum ($\Delta\nu$) of the resonance as shown in Fig. 6(a). The Q-factor is then calculated using $Q = \nu/\Delta\nu$ where ν is the resonant frequency. For ultra-high Q-factors, the cavity ringdown appears to be more suitable. Fig. 6(b) shows a ringing spectrum when the probe laser frequency is scanned fast enough in a prism-coupled WGM resonator made of barium fluoride (BaF_2) [69]. The scanning speed was set at 0.32 THz/s. A theoretical model described in Ref. [72] was used to fit the data. Most WGM resonators have a quality factor above 10^6 at the telecom wavelength of 1550 nm, and billion quality factors are also routinely achieved with mm-size resonators made with metal difluoride crystals [70,73–82].

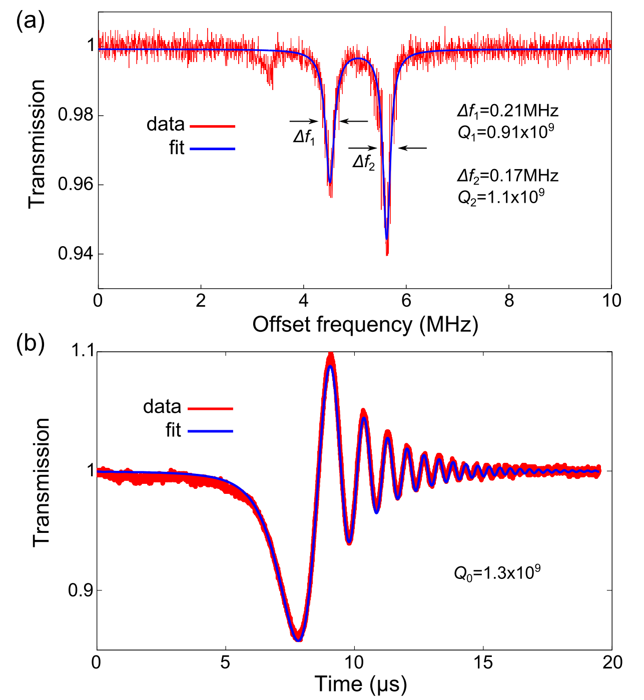

Fig. 6. The measurement techniques for Q factors above one billion in a WGMR: (a) Linewidth measurement in the under-coupling regime. (b) Ringing measurement with fast frequency sweep. Adapted with permission from Ref. [69], © 2014 Optical Society of America.

2.2.4. WGM identification with excitation mapping

WGMs are characterized by three mode numbers (q, ℓ, m) and two perpendicular polarization directions (TE and TM). The number q is related to the number of intensity maxima in the radial direction. The numbers ℓ and $m = 0, \pm1, \pm2... \pm \ell$ are the azimuthal and angular mode numbers, respectively, where ℓ is related to the number of TIRs within one round-trip. One can define a polar mode number $p = \ell - |m|$ which corresponds to $p + 1$ intensity maxima in the polar direction. It is thereby important to identify the fundamental WGM ($q = 1$ and $p = 0$), as it features the smallest mode volume and it more likely to enhance the interaction between laser light and matter. However, it is not always easy to locate $q = 1$ modes. Nevertheless, one can use an excitation mapping method to locate the fundamental polar order WGMs [83,84].

Fig. 7 shows the excitation mapping result of a silica microsphere on a fiber tip and a silica microtoroid on an silicon chip [83]. A sub-micrometer diameter tapered fiber mounted on a three dimensional translation stage with nanometer precision is used to excite the resonator. The sub-wavelength tapered fiber was fabricated using a butane microtorch [57]. The coupling efficiency of the fiber-coupled WGM resonator relies on the internal field distribution of the cavity modes. In a spherical cavity, the intensity distribution in the polar direction of the lightwave is determined by the spherical harmonic $|Y_\ell^{\ell-p}|^2$. Therefore, the spatial mapping of the coupling efficiency for a selected mode corresponds to the polar mode number p. In the fiber-coupled microsphere setup as shown in Fig. 7(a and b), the scanning of the fiber coupler is set in the vertical direction. The polar mode numbers of the WGMs are then revealed by plotting a waterfall figure. For the microtroid setup, this is done using a curved scanning path as

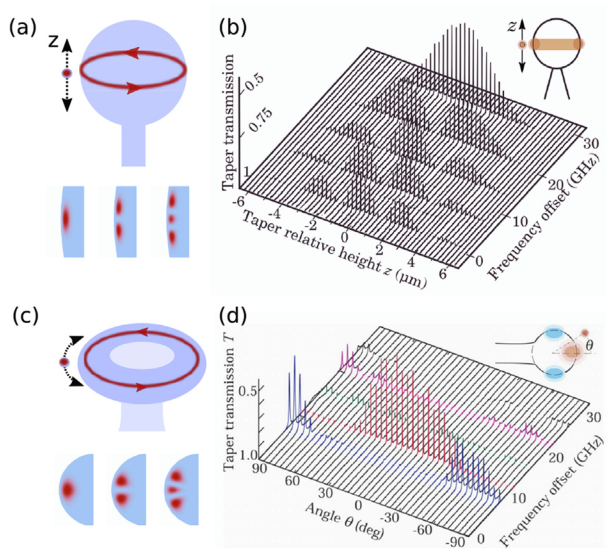

Fig. 7. The excitation mapping technique for recognizing WGMs: the side view illustration of a tapered fiber coupler moving in the vicinity of a silica microsphere WGMR in the vertical direction (a) and a silica microtoroid WGMR in the angular direction (c). (b,d) Waterfall plot of the mapping results for the microsphere and the microtoroid respectively. Adapted with permission from Ref. [83], © 2010 Optical Society of America.

shown in Fig. 7(c and d).

2.2.5. *Thermal bistability based probing method*

The probed spectral shape of an optical resonance in a WGM resonator is usually Lorentzian. However, it can be distorted as a result of thermal bistability [85,86]. If we consider the case of a taper-coupled silica resonator which has a positive thermo-optical coefficient, a fraction of the laser power is absorbed by the cavity as the frequency of the laser approaches the center frequency of a resonant mode from the blue side (the shorter wavelength side). The generated heat leads to a downshift of the resonant frequency, thereby following the laser frequency sweeping direction. The line shape is then broadened as shown in Fig. 8 and vice-versa in the opposite case [86]. Note that in slow timescales, the thermal expansion effect should also be taken into account as an opposite sign of this coefficient can result in thermal oscillations. The oscillation time scales can be in the order of 1 s for millimeter-size WGM resonators [87]. On the other hand, self-thermal locking can occur when signs of the thermal-expansion coefficient and the thermo-optical coefficent are same [86]. It is important to note that beside thermal effects, the WGM resonances can also be shifted by mechanical stresses, such as those induced by the resonator mounting [88].

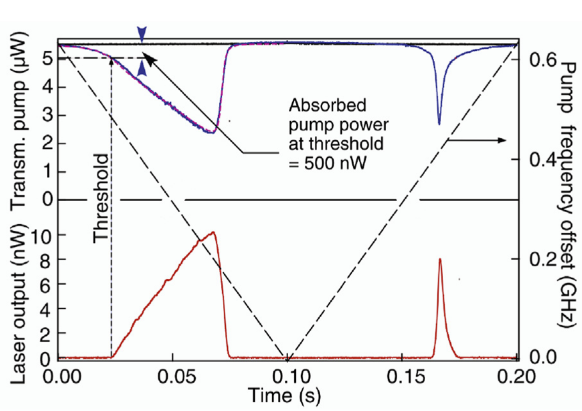

Fig. 8. The thermal bistability phenomenon utilized for fast WGMR microlaser characterization. Adapted with permission from Ref. [86], © 2012 Optical Society of America.

Fig. 8 shows an application of thermal bistabiliy for the characterization of a microsphere laser [86]. As the excited resonant shape is distorted, the coupled laser power into the resonator varies slowly in the broadened side. This window can thereby be used to examine the threshold and the slope efficiency of the laser in a fast timescale. Self-thermal locking when the laser frequency is fixed has also been used to verify the validity of this method [86]. Note that self-thermal locking and thermal bistability are also frequently used in Kerr frequency comb generation and helps to monitor the onset regime for soliton generation [31].

3. Rare-earth lasers

We have introduced the basics of traditional TIR MRRs and WGMRs in the preceding section. Here we briefly review some of the most important applications of these MRRs in laser systems.

It is known that high *Q*-factors and small mode volumes can enhance the light fields in the resonator and thus greatly reduce the threshold pump power. Another important characteristic is that narrow-linewidth lasing can be facilitated by high *Q*-factors. The fundamental laser linewidth limit is given by the Schalow-Townes equation [89] $\Delta\nu_L = 2\pi h\nu(\Delta\nu_r)/P_{\rm out}$, where $h\nu$ is the photon energy and $\Delta\nu_r$ is the linewidth of resonance mode which is inversely proportional to *Q*. If we consider a *Q* factor of 10^8 for a cold MRR at 1064 nm and an output power of 1 mW, the fundamental linewidth limit would be 9 mHz. Note that the fundamental linewidth limit above laser threshold is two times smaller and is known as the modified linewidth equation [90].

Rare-earth lasers can involve three or four energy levels, and Fig. 9 illustrates the generic energy diagrams of three-level and four-level lasers [89]. The transitions related to pumping and lasing energy levels are highlighted as solid arrows together with non-radiative relaxation in dashed arrows. In this section, we will review rare-earth based lasers developed using NPROs and WGMRs from the aspect of materials either as host or surface functionalization.

3.1. *NPRO*

A very important development of TIR MRRs-based lasers is the nonplanar ring oscillator invented by Kane et al. in 1985 [91]. It has become a well-known commercial high-coherent continuous-wave (cw) laser source. A typical geometry of an Nd:YAG NPRO is shown in Fig. 2 (b) with three TIRs and one reflection on a coated surface for free space coupling [92]. The light path in one round-trip does not lie on one plane. A nonplanar structure is formed by reflections on tilted surfaces, so as to create loss differences between clockwise and counter-clockwise modes with the presence of a magnetic field due to the Faraday effect. More details on this concept can be found in Ref. [93]. The successful application of NPROs covers various areas where high-coherence and rigidity is required. To date, NPROs have been chosen as laser sources in gravitational wave detection on ground in LIGO, and in the LISA Pathfinder satellite mission in space [94,95], amongst other projects. NPROs have used various YAG materials, such as Nd:YAG, Yb:YAG, Ho:YAG, Tm:YAG, Er:YAG, in order to generate narrow-linewidth lasers at other frequencies [91,92,96–105].

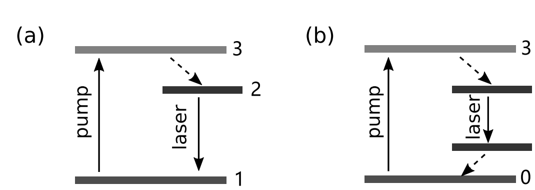

Fig. 9. Energy-level diagrams of rare-earth materials for three-level laser (a) and four-level laser (b).

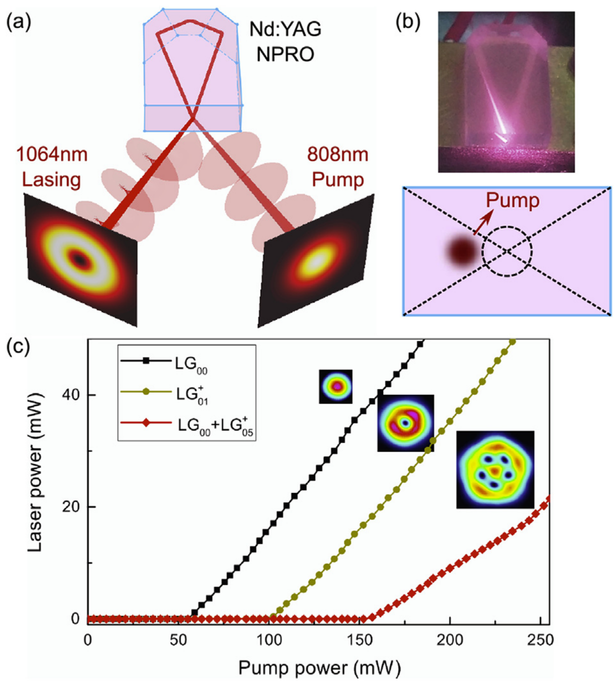

Fig. 10. Lasing in an Nd:YAG NPRO: (a) Illustration of the vortex laser. (b) Photograph of the Nd:YAG NPRO with laser on action (top) and a schematic drawing of off-axis pumping (bottom). (c) Lasing characterization for a fundamental Gaussian beam, a Laguerre-Gaussian beam and a vortex-crystal beam. Adapted with permission from Ref. [92], © 2019 Optical Society of America.

It was recently reported that narrow-linewidth beams carrying orbital angular momentum (OAM) can be directly generated using an NRPO platform [105]. OAM of light has been attracting significant interest in recent years due to its applications in superesolution microscopy, high capacity optical communication, optical manipulation and quantum optics [106,107]. Fig. 10(a) illustrates the schematic of the monolithic OAM emitter at 1064 nm pumped by a Gaussian beam at 808 nm. A photography of this laser in operation is presented in Fig. 10(b). The round-trip path of the laser beam was recorded by a camera. The emission of Laguerre-Gaussian beams was realized by off-axis pumping to selectively excite the high-order modes in the NPRO. It should be noted that nonplanar ring optical resonators based on four mirrors have also been used to study quantum dynamics in synthetic Landau levels for photons [108].

Moreover, spatially distributed crystal-like OAM was found as a result of superposition of different Laguerre-Gaussian (LG) modes [92]. The lasing power curves as a function of the pump power are plotted in Fig. 10(c) for the fundamental Gaussian mode, the LG_{01} mode and the vortex crystal mode lasing. Fig. 11 shows a typical narrow linewidth beat note of a laser beam carrying vortex crystals. It was obtained by beating with a commercial narrow-linewidth reference laser. A 3 dB linewidth of 2 kHz was recorded. The inset shows the spectrum of the scanning Fabry-Perot (FP) signal indicating single-frequency operation.

3.2. WGMR

WGM resonators generally feature better Q factors and smaller mode volumes in comparison to NPROs. Therefore, these resonators are expected to enable ultra-low threshold lasing in the microwatt or even nanowatt regime [43,45]. An extended literature has been devoted to investigate various functional materials including rare-earth, metal, organic and semiconductor materials using the WGMR platform (recent works include for instance, Refs. [109–136]).

Rare-earth materials are particularly important for in solid-state laser technology. For example, stimulated emission in a rare-earth

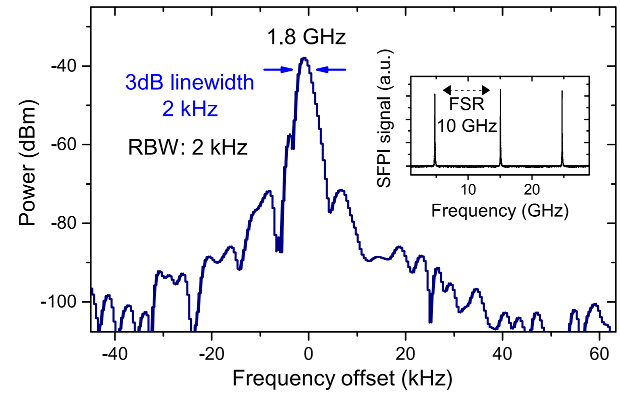

Fig. 11. Typical single frequency beating signal featuring a resolution limited 2 kHz linewidth by mixing it with a reference laser. Inset: the transmitted signal from a scanning Fabry-Perot interferometer. Adapted with permission from Ref. [92], © 2019 Optical Society of America.

WGM resonator was demonstrated soon after the invention of the laser [139]. The laser gain material can be directly doped into host materials such as crystals, fused silica, or ZBLAN glasses [43,45,140]. Another approach is to functionalize the surface of the cavity by coating or embedding with a layer of gain materials. A typical example is through sol-gel coating. Fig. 12(a and b) shows photographs of silica microspheres coupled with a tapered silica fiber by pumping at 980 nm [137]. The visible green light originates from upconverted photons coupled into WGMs with different polar mode numbers p. The threshold power is found to be in the order of tens of μW, as shown in Fig. 12(c).

A continuous-wave threshold at room temperature as low as 200 nW was reported by Sandoghdar et al. in 1996 using a prism-coupled neodymium-doped silica microsphere [141]. In 2010, Lin et al. demonstrated a single mode lasing with threshold down to 65 nW [138].

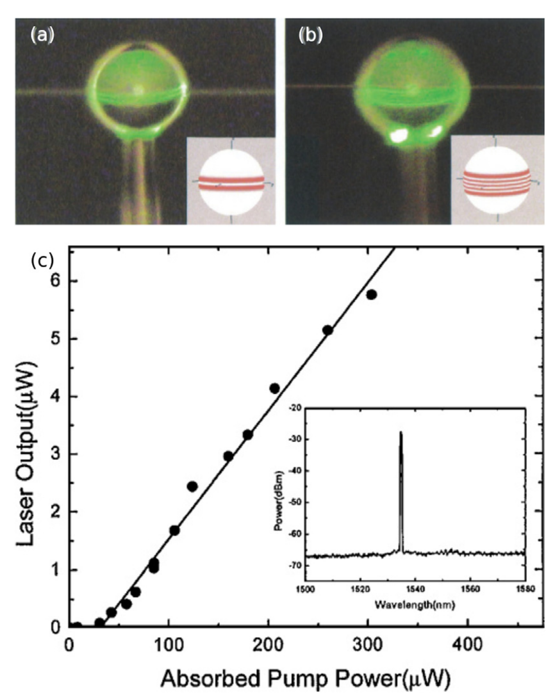

Fig. 12. (a,b) Photographs of the silica microsphere WGMR functionalized with Er-doped solgel films with different modes excited by a tapered fiber. The green color results from the upconverted luminescence. (b) The laser output power as a function of the absorbed pump power. Inset: Lasing spectrum. Adapted with permission from Ref. [137], © 2003 Optical Society of America. (For interpretation of the references to color in this figure legend, the reader is referred to the Web version of this article.)

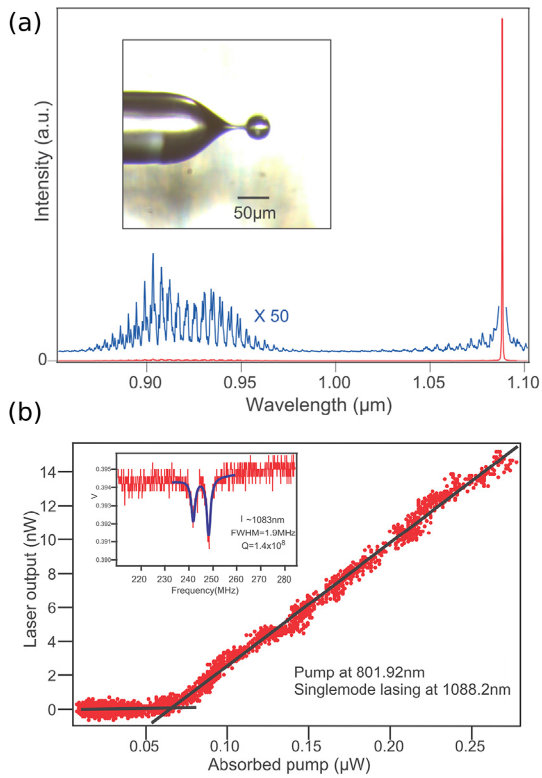

Fig. 13. Microsphere WGMR laser functionalized through Nd-doped Gd_2O_3 core-shell nanocrystals embedding. (a) The lasing spectrum with the pump power near the threshold. Inset: a photograph of the microsphere fabricated in a tapered fiber tip. (b) The laser power as a function of the absorbed pump power showing a cw pump power threshold of about 65 μW. Adapted with permission from G. Lin et al. Proc. SPIE 7716, 771622 (2010) [138].

The silica microsphere was coated with core-shell nanocrystals (core: Nd^{3+}:Gd_2O_3, shell: silica) and further annealed with a CO_2 laser beam. A tapered fiber was used to couple the pump laser at 808 nm in and the lasing signal out from the cavity. Fig. 13(a) shows the photograph of the microsphere fabricated on the tip of a single mode fiber. Also shown is the emission spectrum slightly above lasing threshold. The zoom-in of the spectrum is offset in order to allow for a comparison between the lasing modes and the luminescent modes. One can see that the photoluminescence (PL) was coupled into WGMs and also featured narrow linewidth peaks in the spectrum. Nevertheless, the lasing mode stood out in comparison to PL modes and its power increased linearly above threshold. In contrast, the power of the PL modes actually turned to be saturated above the threshold pump power due to the gain competition with lasing modes as reported in Ref. [86]. Fig. 13(b) shows the recorded ultralow-threshold operation using the thermal bistability effect introduced previously [86]. The inset shows the measured cold cavity linewidth, which is in the order 10^8 for the functionalized cavity around the lasing wavelength, indicating no clear degradation of Q-factor during the functionalization with nanoemitters.

4. Non-centrosymmetric materials for nonlinear photonics

The specific properties of MRRs not only favor the application in rare-earth laser developments, but also facilitate the investigation of nonlinear photonics using cw lasers operating in the low power regime (mW or lower) [30]. It is therefore interesting to study TIR MRRs made from non-centrosymmetric materials, in order to benefit from their intrinsic second-order nonlinearity. Note that WGM resonators have been used to study second-harmonic generation in centrosymmetric materials with molecular surface layers [142] or using an asymmetric cavity [143]. Here, we mainly review the application of crystalline MRRs,

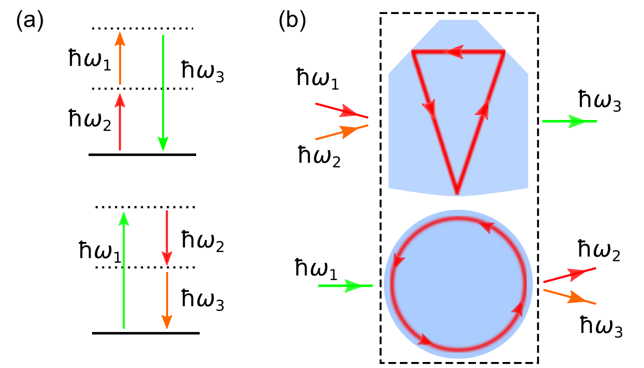

Fig. 14. Illustration of three-wave mixing phenomena: (a) Energy-level diagrams. (b) Resonance enhanced second-harmonic effect utilizing TIR based MRRs and WGMRs.

which are characterized by their much larger nonlinearity and thus better conversion efficiency.

The nonlinear optical effects originate from the polarization response of dielectric materials in the presence of an intense laser beam electric field [144,145]. The polarization dependence at the atomic scale on the electric field can be expanded in power series following $\mathbf{P} = \mathbf{P}^{(1)} + \mathbf{P}^{(2)} + \mathbf{P}^{(3)}$, with $\mathbf{P}^{(1)}$ being the linear term, and $\mathbf{P}^{(2,3)}$ being the nonlinear terms. The second-order nonlinear term is expressed as $\mathbf{P}^{(2)} = \varepsilon_0\chi^{(2)}\mathbf{EE}$, where ε_0 is the permittivity of free space, $\chi^{(2)}$ is the second-order nonlinear susceptibility and $\mathbf{E}$ is the electric field of the light beam. The $\chi^{(2)}$ tensor is actually non-zero only for non-centrosymmetric optical materials. This second order term is responsible for various three-wave mixing (TWM) effects. Fig. 14(a) illustrates two types of TWM processes in the energy level diagram with dashed lines as virtual energy levels. TWM is a parametric process in which two photons can be converted into one photon, provided that energy and momentum are conserved, such as in second-harmonic generation (SHG) and sum-frequency generation (SFG). Reversely, one photon can also be down-converted into two photons, a process which is known as optical parametric oscillation (OPO) above threshold. Such effects can be amplified using single- or multiple-resonant enhancement in MRRs as shown in Fig. 14(b).

The momentum conservation law imposes a strict phase-matching requirement for efficient TWM processes. For a typical macroscopic MRR, non-critical phase matching is often used in a z-cut geometry as shown in Fig. 15(a), for which the temperature is usually set to an optimal point where the material dispersion is such that the phase-matching condition is fulfilled. In WGM resonator platforms, three main phase-matching techniques have been demonstrated so far. The traditional phase-matching methods used in bulk crystals such as non-critical phase-matching (NCPM) and quasi-phase-matching (QPM) can be

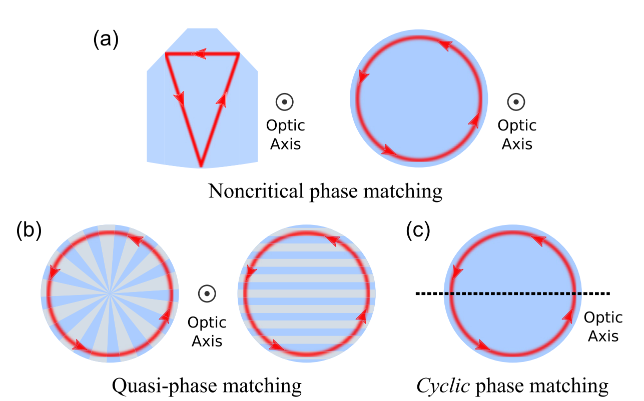

Fig. 15. Three phase-matching techniques for monolithic ring cavities: (a) Noncritical phase-matching, (b) Quasi-phase-matching (radial and linear poling), (c) *Cyclic* phase-matching.

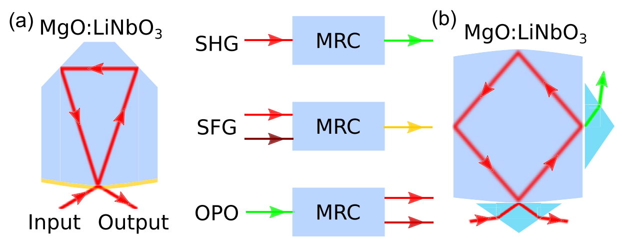

Fig. 16. Illustration of reported nonlinear frequency conversion using TIR based MRRs made from lithium niobate: (a) HR coating for free space coupling and (b) Full TIRs with prism coupling. SHG: second-harmonic gereration. SFG: sum-frequency generation. OPO: optical parametric oscillation.

employed as illustrated in Fig. 15(a and b). Both radial and linear poling can be applied in WGM resonators made from ferroelectric materials [30,47]. A new phase-matching method was developed in the WGMR platform by Lin et al. with an x-cut BBO disk in 2013 [146,147]. Fig. 15(c) shows the scheme of this geometry where the optic axis lies on the disk plane leading to a special WGM with oscillatory refractive index upon propagation. Further details will be discussed in the section devoted to beta barium borate crystals.

4.1. Lithium niobate ($LiNbO_3$)

Lithium niobate ($LiNbO_3$) is widely used in integrated photonics and in the IR regime for applications based on second-order nonlinearities. As far as $LiNbO_3$ resonators are concerned, early research has been carried out using mechanically polished TIR MRRs with triangular or rectangular round-trip paths as illustrated in Fig. 16. Note that non-critical phase-matching (NCPM) is often used in such cavities for efficient nonlinear optical processes including SHG, SFG and OPO, which typically require working temperature above 100 °C. High conversion efficiency with cw pump power has been reported in several research works [148–153]. For instance, 65% conversion efficiency was reported with 310 mW pump power at 1064 nm [148]. OPO threshold in the regime of sub-W was successfully achieved as well. Conversion efficiency exceeding 5% with pump power above 5 mW was also demonstrated using a fully TIR monolithic resonator [150]. Two $CaCO_3$ prisms with perpendicular optic axis orientations were used to selectively incouple the fundamental frequency and out-couple the second-harmonic from the cavity as illustrated in Fig. 16(b). Recently, precision diamond turning was also used in fabricating this type of nonlinear cavities for squeezed light generation [153].

TWM phenomena in $LiNbO_3$ WGM resonators have also been widely investigated both theoretically and experimentally [29,30,47]. In mm-size WGM resonators, Q above 10^8 and QPM-based efficient SHG in periodically poled $LiNbO_3$ (PPLN) have been reported in 2004 [154]. Efficiency as high as 9% with only 30 μW cw pump power at 1064 nm was demonstrated by using non-critical phase-matching in a $LiNbO_3$ disk in 2010 [155]. Cyclic phase-matching as developed by Lin et al., in 2013 [146] was also applied for $LiNbO_3$ WGM resonators in both μm and mm-size cavities [156,157]. The same cavity configuration was recently used for natural quasi-phase-matching in $LiNbO_3$ microdisks [158]. It should be noted that the resonance-enhanced TWM processes also include SFG, OPO and other cascaded effects [159–166]. In the case of microscale $LiNbO_3$ WGM resonators, several works have reported progress on the technology of high-Q, on-chip $LiNbO_3$ microdisks [156,167–174]. The fact that mm-size lithium niobate WGM resonators can be polished in both x- and z-cut also makes them suitable for several applications in photonics where these optical anisotropies are of specific interest [175].

4.2. Beta barium borate

Along with $LiNbO_3$, beta barium borate (BBO) is a commonly used

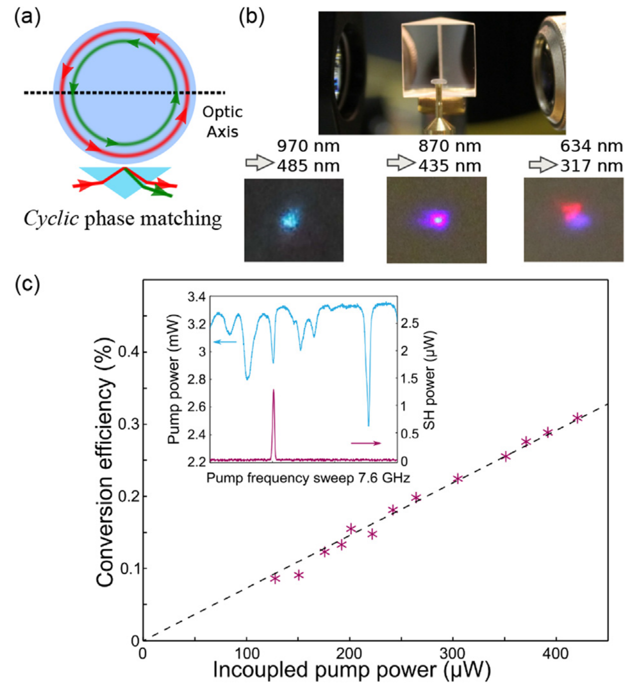

Fig. 17. *Cyclic* phase-matched wide range second harmonic generation in a high-Q BBO WGMR. (a) Illustration of the prism-coupled x-cut BBO WGMR with the optic axis parallel to the disk plane. (b) Photograph of the setup. (c) The conversion efficiency of second harmonic generation into UV wavelength of 317*nm* as a function of the incoupled pump power. Inset: typical scanning WGMR spectrum at the pump wavelength and the monitoring of the harmonic signal. Reprinted with permission from Ref. [146], with the permission of AIP Publishing.

nonlinear crystal, which has relatively large nonlinear coefficient and wide transparency window into the ultra-violet (UV) regime. BBO WGM resonators can feature high Q-factors, in the order of 10^8 at 370 nm [146]. However, BBO is a non-ferroelectric material, thereby not suitable for periodic poling. As a result, phase-matching was then explored by investigating symmetry breaking in a non-z-cut BBO WGMR [146,147,176]. Birefringence is another property of this crystal that strengthens the interest of the scientific community for such geometries. For example, it was shown that high-Q WGMs only exist as ordinarily polarized modes in angle-cut BBO WGM resonators, when the optic axis is tilted from the symmetric axis of the disk. Consequently, light waves were found to feature a rotating polarization orientation upon propagation in a high-Q WGM [176].

On the other hand, laser light propagation in a WGM featuring an oscillatory refractive index alternating from ordinary to extraordinary upon propagation in an x-cut BBO was demonstrated in 2013 [146]. Fig. 17(a) depicts such an x-cut geometry for SHG in a BBO disk. Perfect phase-matching points can be found within one round-trip covering a wide spectral range, leading to the so called *cyclic* phase-matching [146]. As shown in Fig. 17(b and c), SHG with fundamental wavelengths from visible to infrared was demonstrated as well, and further details can be found in Ref. [146]. Broad tuning of a UV laser from the BBO WGM doubler was also realized by combining both stress and temperature tuning methods [147].

4.3. Other materials

WGM resonators have emerged as an ideal platform to explore not only fundamental material properties, but also their application for generating laser sources in new spectral windows. Macroscopic crystalline WGM resonators have been fabricated from various other materials including lithium tetraborate, lithium tantalate and $CdSiP_2$ for

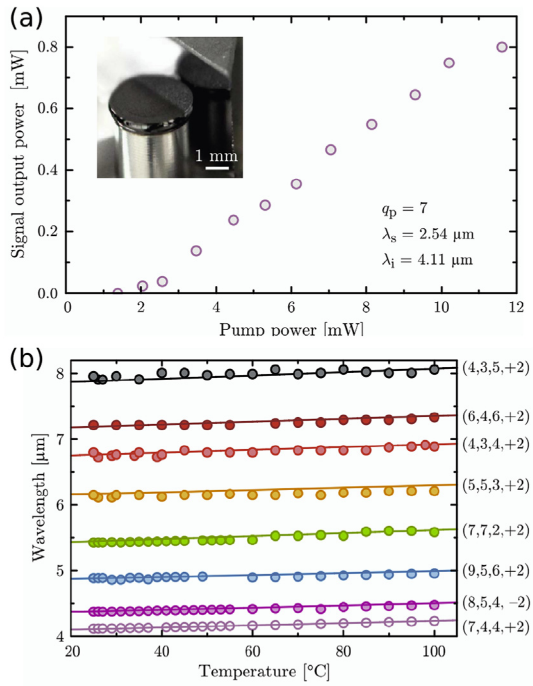

Fig. 18. Optical parametric oscillation from a crystalline WGMR made of $AgGaSe_2$. (a) OPO signal output at 2.54 μm versus the pump power at 1.57 μm. Inset: photo of the silicon prism coupled WGMR. (b) The idle wavelengths versus the temperature of the cavity with theoretical curves. Reprinted with permission from Ref. [183]. © 2017 Optical Society of America. (For interpretation of the references to color in this figure legend, the reader is referred to the Web version of this article.)

SHG into UV or OPO into the mid-infrared (mid-IR) regime [166,177–186]. For instance, a high-Q $AgGaSe_2$ WGMR coupled by a silicon prism was used to generate mid-IR lasers up to 8 μm [183]. Fig. 18(a) presents an example of the signal output power as a function of the pump power, showing cw threshold power in the mW regime. The temperature tuning curves are given in Fig. 18(b).

5. Centrosymmetric materials for nonlinear photonics

Although second-order nonlinearity is typically only present in non-centrosymmetric materials, the third-order nonlinearity does not require special symmetries. It is related to the third nonlinear polarization term of the material in response to the electric field of a light beam, following $\mathbf{P}^{(3)} = \varepsilon_0 \chi^{(3)} \mathbf{EEE}$ where $\chi^{(3)}$ is the third-order nonlinear susceptibility of the material. The corresponding nonlinear photonic effects with WGM resonators are illustrated in Fig. 19. Fig. 19(a) depicts four-wave mixing (FWM) processes in a WGM resonator. Such effects include third-harmonic generation (THG) and regular FWM, whose energy diagrams are given in Fig. 19(b and c), respectively. As illustrated in Fig. 19(d), other types of third-order nonlinear optical effects are stimulated Raman scattering (SRS) and stimulated Brillouin scattering (SBS), which involves the interaction of photons with optical or acoustic phonons. The energy diagrams of Stokes and anti-Stokes waves with creation and annihilation of phonons are shown in Fig. 19(e and f), respectively.

5.1. Fused silica

A quite common optical material for TIR based MRRs is fused silica. Due to the mature fabrication techniques for high-purity silica for low-loss optical fibers, ultra-high Q WGM resonators above 10^9 in the visible and near IR regimes have been demonstrated early in silica WGM microsphere resonators [63,64]. Such cavities can be fabricated using surface tension induced by heating with a flame or a laser. Traditional mechanically polished fused silica TIR MRRs featuring Q around 10^8 have also been reported [38]. To date, various types of ultra-high Q WGM resonators made from fused silica have been demonstrated, including microspheres, microtoroids and microbottles. Several research works have been carried out using fused silica WGM resonators in areas such as opto-mechanics, microlasers, sensors and nonlinear photonics [187–213].

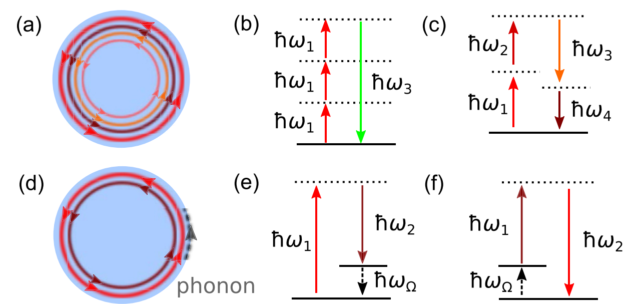

Fig. 19. Typical nonlinear frequency conversion phenomena in in WGM resonators made from centrosymmetric materials. (a) Illustration of traveling light waves in WGM resonators. (b,c) Energy-level diagrams of third harmonic generation and four-wave mixing. (d) Illustration of WGM resonators in presence of phonons. (e,f) Energy-level diagrams of stimulated light-photon scattering processes: (Stokes and anti-Stokes).

An illustration of THG as a nonlinear optical effect is presented in Fig. 20, using a fused silica microtoroid with a cw pump power less than 300 μW at telecom wavelength. Sum-frequency generation based on the third-order nonlinearity of fused silica was also reported in Ref. [191]. Recently, THG was also investigated with increased fiber coupling using a deformed WGMR resulting from chaos-assisted momentum transformation [143]. The finesse of these cavities can exceed 10^6 in a silica micro-WGMR with Q above 10^8. As a result, intense light field can be built up even with a very low pump power in the μW regime. These WGMR platforms have thereby been used to investigate very low threshold SRS and SBS phenomena [30].

An important discovery based on FWM in WGM resonators is the generation of Kerr frequency combs with single frequency laser pumping [192]. Fig. 21(a) displays a Kerr comb spectrum generated using a chipscale silica microtoroid [192]. The energy diagrams of degenerate and non-degenerate FWM are given in Fig. 21(b) and (c), respectively, along with a photograph of the cavity. Note that cascaded effects combined with other nonlinear optical effects such as SRS, SHG and THG have been observed as well [199–203]. Important applications of such microcavity combs have been recently demonstrated in the areas of microwave photonics, spectroscopy and laser ranging [28,31–33]. It should also be noted that ultra-high Q WGM resonators

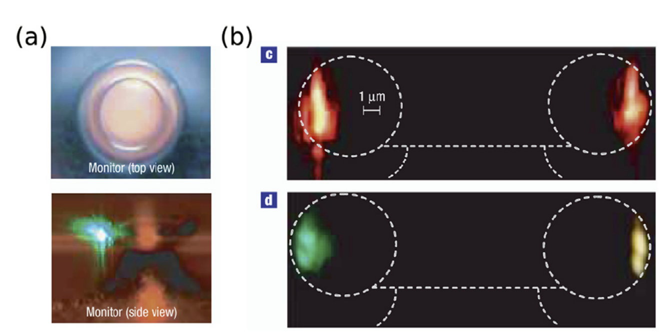

Fig. 20. Third-harmonic generation in silica microcavities. (a) Photographs of a silica microtoroid coupled with a tapered fiber. (b) Photographs of the nonlinear cavity with two pump lasers in counter-rotating directions: same lasers (top), different lasers (bottom). Reprinted by permission from Macmillan Publishers Ltd.: Carmon et al. Nat. Phys. 3, 430 (2007) [191]. Copyright 2007.

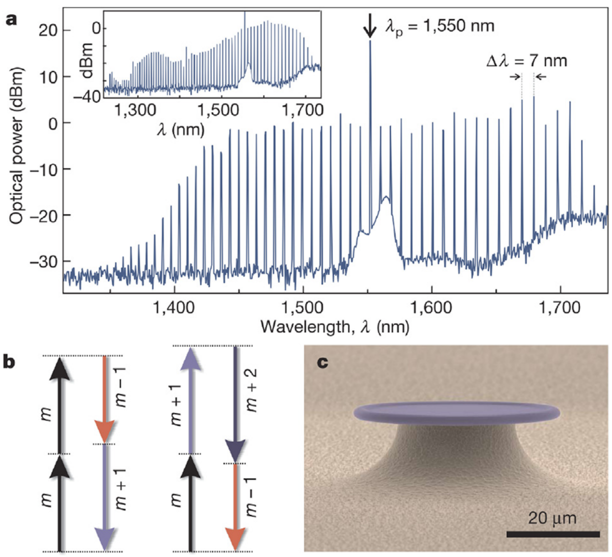

Fig. 21. Kerr optical frequency comb generation in a silica microtoroid on-chip. (a) The optical spectrum, (b) Energy-level diagram, (c) Image of the cavity. Reprinted by permission from Macmillan Publishers Ltd.: Del'Haye et al., Nature 450, 1214 (2007) [191]. Copyright 2007.

can be fabricated with fused quartz as bulk material [214].

5.2. Fluoride crystals

Fluoride crystals are very popular optical materials for the fabrication of WGM resonators. They usually feature high transparency in the spectral range covering from UV to mid-IR, often used as optical windows. However, crystal lattices can be broken if one tries to use surface tension methods to form a high-Q crystalline WGM resonator. Therefore, ultra-high-Q crystalline WGM resonators are generally produced using mechanical polishing techniques [215]. The highest Q is in the order of 10^{11}, and it was reported in a CaF_2 WGM resonator [67]. To date, fluoride WGM resonators have been produced and investigated from crystals including CaF_2, MgF_2, BaF_2, SrF_2 and LiF crystals (see for example refs [66,154,216–228]). Such WGM resonators can be used to provide narrow linewidth lasers using self-injection locking technique based on Rayleigh scattering [124,229,230].

The Raman gain bandwidth is typically several orders of magnitude larger than that of the Brillouin gain, even though gain coefficient is smaller. For this reason, SRS tends to be easier observed in WGM resonators [231]. Interestingly, phase-locked Raman combs with one and multiple-FSR spacing in the normal dispersion regime was recently reported with BaF_2 WGM resonators [81]. With respect to the SBS effect [232], precise Brillouin frequency shift matching single or multiple-FSR was generally the preferred strategy to achieve Brillouin lasing, using the high-Q modes that appear in the gain profile [217]. It was latter reported that cascaded Brillouin lasers can still be generated in a large mm-size WGM resonators, which favors rich multimode structures [221]. A recent theoretical study has found that BaF_2 WGM resonators with proper orientation along [111] feature small variation of Brillouin shift upon intracavity propagation, and therefore, BaF_2 is expected to be a particularly suitable crystal for Brillouin lasing among these fluorides [233].

It should also be noted that the ultra-high Q factors that can be achieved with fluorite crystals have been one of the key property that has led to the emergence of the science and technology of Kerr optical frequency combs. This topic has been thoroughly investigated experimentally, but has also been the focus of an extended body of literature from the theoretical viewpoint (see for example refs. [234–240] and references therein). Beyond Kerr comb generation, the large crystalline

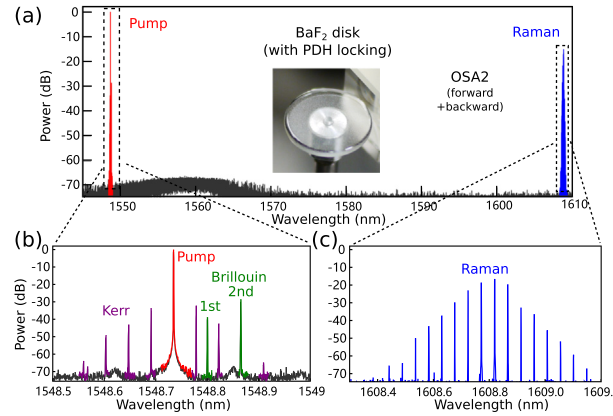

Fig. 22. Universal nonlinear scattering in a crystalline WGM resonators made from BaF_2 involving SRS, SBS and FWM processes simultaneously. (a) The optical spectrum and a photo of the SF11 prism coupled BaF_2 disk. (b,c) The zoom-in optical spectra in the pump and Raman spectral windows, respectively. Adapted with permission from Ref. [227], © 2016 Optical Society of America.

WGM resonators also provide an ideal platform to study the interaction of photons with matter scaling from electronic to lattice levels. Simultaneously, generation of stable SRS, SBS together with FWM combs can be easily created by pumping a fluoride WGMR with one billion Q factors, and this phenomenon has been referred to as universal nonlinear scattering [227]. Fig. 22(a) shows the optical spectrum pumped by a locked laser with few tens of mW at the telecom wavelength of 1550 nm around the pump and the Raman lasing components are presented in Fig. 22(b and c). One can clearly observe the Brillouin laser lines, Raman comb lines and the Kerr comb lines. Note that triple combs around the pump, Brillouin Stokes and anti-Stokes were also reported in a SrF_2 disk [227].

5.3. Other materials

Other centrosymmetric materials have also been explored using ultra-high Q WGMR platforms. For instance, a diamond WGMR was demonstrated with Q factors in the order of 10^7, limited by the purity of the single-crystal diamond synthesized using chemical vapor deposition [59,241]. Recently, Q factors above one billion in silicon WGM resonators at the telecom wavelength was also reported [60]. Similar Q factors have also been demonstrated in WGM resonators made from quartz and sapphire crystals [65,68]. Photonic systems based on chalcogenide compounds have been reported [242,243]. Many other materials can also benefit from WGMR platforms either by changing the entire host material or through surface coating [244–247]. Combined with particular advantages of these optical materials, such WGM resonators can find potential applications in sensors, telecommunications and metrology.

6. Conclusion

We have briefly reviewed the development of traditional TIR MRRs and WGM resonators for photonics applications. Their long-lifetime photon-trapping capability and in-built nonlinearity has permitted these devices to be at the center of various systems, including narrow-linewidth Gaussian and vortex laser beams, rare-earth solid-state lasers, optical frequency converters, Brillouin lasers, Raman lasers, Kerr optical frequency combs, just to name a few.

Even though the literature related to the principles and applications of these resonator is already quite large, there are indeed several avenues for future research on this topic. A straightforward challenge is to achieve a better theoretical understanding of the phenomena that are induced by the laser-matter interaction, including at the quantum level

[248]. Major advances have been achieved in the context of Kerr comb generation, but the other nonlinear interactions have not benefited from the same attention from the scientific community. The second objective is to develop systems with performances that are competitive with existing or alternative technologies. The preliminary results so far are indeed encouraging but the leap from the laboratory to commercial products requires to optimize many parameters such as power efficiency, robustness and stability.

Acknowledgements

Guoping Lin would like to thank the National Natural Science Foundation of China (grant no. 61605051). Yanne K. Chembo acknowledges financial support from the University of Maryland.

References

[1] N. Hodgson, H. Weber, Laser Resonators and Beam Propagation: Fundamentals, Advanced Concepts, Applications vol. 108, Springer, 2005.
[2] M. Sumetsky, Y. Dulashko, J.M. Fini, A. Hale, D.J. DiGiovanni, The microfiber loop resonator: theory, experiment, and application, J. Light. Technol. 24 (2006) 242–250.
[3] D.G. Rabus, Integrated Ring Resonators, Springer Series in Optical Sciences, 2007.
[4] D. Liang, J.E. Bowers, Recent progress in lasers on silicon, Nat. Photon. 4 (2010) 511.
[5] W. Bogaerts, P. De Heyn, T. Van Vaerenbergh, K. De Vos, S. Kumar Selvaraja, T. Claes, P. Dumon, P. Bienstman, D. Van Thourhout, R. Baets, Silicon microring resonators, Laser Photonics Rev. 6 (2012) 47–73.
[6] X. Guo, C.-L. Zou, H.X. Tang, Second-harmonic generation in aluminum nitride microrings with 2500%/W conversion efficiency, Optica 3 (2016) 1126–1131.
[7] A.D. Logan, M. Gould, E.R. Schmidgall, K. Hestroffer, Z. Lin, W. Jin, A. Majumdar, F. Hatami, A.W. Rodriguez, K.-M.C. Fu, 400 W second harmonic conversion efficiency in 14 μm-diameter gallium phosphide-on-oxide resonators, Optic Express 26 (2018) 33687–33699.
[8] J.B. Surya, X. Guo, C.-L. Zou, H.X. Tang, Efficient third-harmonic generation in composite aluminum nitride/silicon nitride microrings, Optica 5 (2018) 103–108.
[9] X. Liu, A.W. Bruch, Z. Gong, J. Lu, J.B. Surya, L. Zhang, J. Wang, J. Yan, H.X. Tang, Ultra-high-Q UV microring resonators based on a single-crystalline AlN platform, Optica 5 (2018) 1279–1282.
[10] R. Luo, Y. He, H. Liang, M. Li, J. Ling, Q. Lin, Optical Parametric Generation in a Lithium Niobate Microring with Modal Phase Matching, (2018) arXiv preprint arXiv:1810.01299.
[11] J.D. Joannopoulos, S.G. Johnson, Winn, N. Joshua, R.D. Meade, Photonic Crystals: Molding the Flow of Light, Princeton university press, 2011.
[12] M. Aspelmeyer, T.J. Kippenberg, F. Marquard, Cavity optomechanics, Rev. Mod. Phys. 86 (2014) 1391–1452.
[13] C. Dong, V. Fiore, M.C. Kuzyk, H. Wang, Optomechanical dark mode, Science 338 (2012) 1609–1613.
[14] Z. Shen, Y.-L. Zhang, Y. Chen, F.-W. Sun, X.-B. Zou, G.-C. Guo, C.-L. Zou, C.-H. Dong, Reconfigurable optomechanical circulator and directional amplifier, Nat. Commun. 9 (2018) 1797.
[15] K. Volyanskiy, P. Salzenstein, H. Tavernier, M. Pogurmirskiy, Y.K. Chembo, L. Larger, Compact optoelectronic microwave oscillators using ultra-high Q whispering gallery mode disk-resonators and phase modulation, Optic Express 18 (2010) 22358–22363.
[16] L. Maleki, Sources: the optoelectronic oscillator, Nat. Photon. 5 (2011) 728–730.
[17] T. Hao, J. Tang, D. Domenech, W. Li, N. Zhu, J. Capmany, M. Li, Toward monolithic integration of OEOs: from systems to chips, J. Light. Technol. 36 (2018) 4565–4582.
[18] K. Saleh, R. Henriet, S. Diallo, G. Lin, R. Martinenghi, I.V. Balakireva, P. Salzenstein, A. Coillet, Y.K. Chembo, Phase noise performance comparison between optoelectronic oscillators based on optical delay lines and whispering gallery mode resonators, Optic Express 22 (2014) 32158–32173.
[19] K. Saleh, Y. Chembo, Phase noise performance comparison between microwaves generated with Kerr optical frequency combs and optoelectronic oscillators, Electron. Lett. 53 (2017) 264–265.
[20] R.M. Nguimdo, K. Saleh, A. Coillet, G. Lin, R. Martinenghi, Y.K. Chembo, Phase noise performance of optoelectronic oscillators based on whispering-gallery mode resonators, IEEE J. Quantum Electron. 51 (2015) 6500308.
[21] A. Coillet, R. Henriet, P. Salzenstein, K.P. Huy, L. Larger, Y.K. Chembo, Time-Domain dynamics and stability analysis of optoelectronic oscillators based on whispering-gallery mode resonators, IEEE J. Sel. Top. Quantum Electron. 19 (2013) 1–12.
[22] K. Saleh, G. Lin, Y.K. Chembo, Effect of laser coupling and active stabilization on the phase noise performance of optoelectronic microwave oscillators based on whispering-gallery-mode resonators, IEEE Phot. J. 7 (2015) 5500111.
[23] L. Feng, R. El-Ganainy, L. Ge, Non-Hermitian photonics based on parity–time symmetry, Nat. Photon. 11 (12) (2017) 752.
[24] M.-A. Miri, A. Alù, Exceptional points in optics and photonics, Science 363 (6422) (2019) eaar7709.
[25] Ş. Özdemir, S. Rotter, F. Nori, L. Yang, Parity–time symmetry and exceptional points in photonics, Nat. Mater. in press, https://doi.org/10.1038/s41563-019-0304-9.
[26] M.R. Foreman, J.D. Swaim, F. Vollmer, Whispering gallery mode sensors, Adv. Opt. Photon 7 (2015) 168.
[27] X. Jiang, A.J. Qavi, S.H. Huang, L. Yang, Whispering Gallery Microsensors: a Review, (2018) arXiv preprint arXiv: 1805.00062.
[28] Y.K. Chembo, Kerr optical frequency combs: theory, applications and perspectives, Nanophotonics 5 (2016) 214–230.
[29] D.V. Strekalov, C. Marquardt, A.B. Matsko, H.G.L. Schwefel, G. Leuchs, Nonlinear and quantum optics with whispering gallery resonators, J. Opt. 18 (2016) 123002.
[30] G. Lin, A. Coillet, Y.K. Chembo, Nonlinear photonics with high-Q whispering-gallery-mode resonators, Adv. Opt. Photon 9 (2017) 828–890.
[31] T.J. Kippenberg, A.L. Gaeta, M. Lipson, M.L. Gorodetsky, Dissipative Kerr solitons in optical microresonators, Science 361 (2018) eaan8083.
[32] A. Pasquazi, M. Peccianti, L. Razzari, D.J. Moss, S. Coen, M. Erkintalo, Y.K. Chembo, T. Hansson, S. Wabnitz, P. DelHaye, et al., Micro-combs: a novel generation of optical sources, Phys. Rep. 729 (2018) 1–81.
[33] J. Wu, X. Xu, T.G. Nguyen, S.T. Chu, B.E. Little, R. Morandotti, A. Mitchell, D.J. Moss, RF photonics: an optical microcombs perspective, IEEE J. Sel. Top. Quantum Electron. 24 (2018) 1–20.
[34] J. Li, M.-G. Suh, K. Vahala, Microresonator brillouin gyroscope, Optica 4 (2017) 346–348.
[35] W. Liang, V.S. Ilchenko, A.A. Savchenkov, E. Dale, D. Eliyahu, A.B. Matsko, L. Maleki, Resonant microphotonic gyroscope, Optica 4 (2017) 114–117.
[36] K. Qian, J. Tang, H. Guo, W. Liu, J. Liu, C. Xue, Y. Zheng, C. Zhang, Under-coupling whispering gallery mode resonator applied to resonant micro-optic gyroscope, Sensors 17 (2017) 100.
[37] A.A. Savchenkov, W. Liang, V. Ilchenko, A. Matsko, L. Maleki, Crystalline waveguides for optical gyroscopes, IEEE J. Sel. Top. Quantum Electron. 24 (2018) 1–11.
[38] S. Schiller, I. Yu, M.M. Fejer, R.L. Byer, Fused-silica monolithic total-internal-reflection resonator, Opt. Lett. 17 (1992) 378–380.
[39] K.J. Vahala, Optical microcavities, Nature 424 (2003) 839–846.
[40] A.B. Matsko, A.A. Savchenkov, D.V. Strekalov, V.S. Ilchenko, L. Maleki, Review of applications of whispering-gallery mode resonators in photonics and nonlinear optics, IPN Prog. Rep. (2005) 142–162.
[41] V.S. Ilchenko, A.B. Matsko, Optical resonators with whispering-gallery modes - Part II: Applications, IEEE J. Sel. Top. Quantum Electron. 12 (2006) 15–32.
[42] A. Matsko, V. Ilchenko, Optical resonators with whispering-gallery modes-part I: basics, IEEE J. Sel. Top. Quantum Electron. 12 (2006) 3–14.
[43] A. Chiasera, Y. Dumeige, P. Feron, M. Ferrari, Y. Jestin, G. Nunzi Conti, S. Pelli, S. Soria, G.C. Righini, Spherical whispering-gallery-mode microresonators, Laser Photonics Rev. 4 (2010) 457–482.
[44] G. Righini, Y. Dumeige, P. Féron, M. Ferrari, G. Nunzi Conti, D. Ristic, S. Soria, Whispering gallery mode microresonators: fundamentals and applications, Riv. del. Nuov. Cimen. 34 (2011) 435–488.
[45] L. He, S.K. Özdemir, L. Yang, Whispering gallery microcavity lasers, Laser Photonics Rev. 7 (2013) 60–82.
[46] H. Cao, J. Wiersig, Dielectric microcavities: model systems for wave chaos and non-Hermitian physics, Rev. Mod. Phys. 87 (2015) 61–111.
[47] I. Breunig, Three-wave mixing in whispering gallery resonators, Laser Photonics Rev. 10 (2016) 569–587.
[48] X.-F. Jiang, C.-L. Zou, L. Wang, Q. Gong, Y.-F. Xiao, Whispering-gallery microcavities with unidirectional laser emission, Laser Photonics Rev. 10 (2016) 40–61.
[49] D. Venkatakrishnarao, E.A. Mamonov, T.V. Murzina, R. Chandrasekar, Advanced organic and polymer whispering-gallery-mode microresonators for enhanced nonlinear optical light, Adv. Opt. Mater. 6 (2018) 1800343.
[50] J. Yu, E. Lewis, G. Farrell, P. Wang, Compound glass microsphere resonator devices, Micromachines 9 (2018) 356.
[51] Y.-D. Yang, M. Tang, F.-L. Wang, Z.-X. Xiao, J.-L. Xiao, Y.-Z. Huang, Whispering-gallery mode hexagonal micro-/nanocavity lasers, Photon. Res. 7 (5) (2019) 594–607.
[52] Q. Song, Emerging opportunities for ultra-high Q whispering gallery mode microcavities, Sci. China Phys. Mech. Astron. 62 (7) (2019) 074231.
[53] J.C. Knight, G. Cheung, F. Jacques, T. Birks, Phase-matched excitation of whispering-gallery-mode resonances by a fiber taper, Opt. Lett. 22 (1997) 1129–1131.
[54] M.L. Gorodetsky, V.S. Ilchenko, Optical microsphere resonators: optimal coupling to high-Q whispering-gallery modes, J. Opt. Soc. Am. B 16 (1999) 147–154.
[55] V.S. Ilchenko, X.S. Yao, L. Maleki, Pigtailing the high-Q microsphere cavity: a simple fiber coupler for optical whispering-gallery modes, Opt. Lett. 24 (1999) 723–725.
[56] M. Cai, O. Painter, K.J. Vahala, Observation of critical coupling in a fiber taper to a silica-microsphere whispering-gallery mode system, Phys. Rev. Lett. 85 (2000) 74.
[57] F. Orucevic, V. Lefèvre-Seguin, J. Hare, Transmittance and near-field characterization of sub-wavelength tapered optical fibers, Optic Express 15 (2007) 13624–13629.
[58] G. Liu, V.S. Ilchenko, T. Su, Y.-C. Ling, S. Feng, K. Shang, Y. Zhang, W. Liang, A.A. Savchenkov, A.B. Matsko, L. Maleki, S.J.B. Yoo, Low-loss prism-waveguide optical coupling for ultrahigh-Q low-index monolithic resonators, Optica 5 (2018) 219–226.
[59] V. Ilchenko, A. Bennett, P. Santini, A. Savchenkov, A. Matsko, L. Maleki, Whispering gallery mode diamond resonator, Opt. Lett. 38 (2013) 4320–4323.
[60] A.E. Shitikov, I.A. Bilenko, N.M. Kondratiev, V.E. Lobanov, A. Markosyan, M.L. Gorodetsky, Billion Q-factor in silicon WGM resonators, Optica 5 (2018) 1525–1528.
[61] G. Lin, R. Henriet, A. Coillet, M. Jacquot, L. Furfaro, G. Cibiel, L. Larger, Y.K. Chembo, Dependence of quality factor on surface roughness in crystalline whispering-gallery mode resonators, Opt. Lett. 43 (2018) 495–498.
[62] D.W. Vernooy, V.S. Ilchenko, H. Mabuchi, E.W. Streed, H.J. Kimble, High-Q measurements of fused-silica microspheres in the near infrared, Opt. Lett. 23 (1998) 247–249.
[63] L. Collot, V. Lefèvre-Seguin, M. Brune, J.M. Raimond, S. Haroche, Very high-Q whispering-gallery mode resonances observed on fused silica microspheres, Europhys. Lett. 23 (1993) 327.

[64] M.L. Gorodetsky, A.A. Savchenkov, V.S. Ilchenko, Ultimate Q of optical microsphere resonators, Opt. Lett. 21 (1996) 453–455.
[65] A.A. Savchenkov, V.S. Ilchenko, A.B. Matsko, L. Maleki, Kilohertz optical resonances in dielectric crystal cavities, Phys. Rev. A 70 (2004) 051804.
[66] I.S. Grudinin, A.B. Matsko, A.A. Savchenkov, D. Strekalov, V.S. Ilchenko, L. Maleki, Ultra high Q crystalline microcavities, Optic Commun. 265 (2006) 33–38.
[67] A.A. Savchenkov, A.B. Matsko, V.S. Ilchenko, L. Maleki, Optical resonators with ten million finesse, Optic Express 15 (2007) 6768–6773.
[68] V.S. Ilchenko, A.A. Savchenkov, J. Byrd, I. Solomatine, A.B. Matsko, D. Seidel, L. Maleki, Crystal quartz optical whispering-gallery resonators, Opt. Lett. 33 (2008) 1569–1571.
[69] G. Lin, S. Diallo, R. Henriet, M. Jacquot, Y.K. Chembo, Barium fluoride whispering-gallery-mode disk-resonator with one billion quality-factor, Opt. Lett. 39 (2014) 6009–6012.
[70] R. Henriet, G. Lin, A. Coillet, M. Jacquot, L. Furfaro, L. Larger, Y.K. Chembo, Kerr optical frequency comb generation in strontium fluoride whispering-gallery mode resonators with billion quality factor, Opt. Lett. 40 (2015) 1567–1570.
[71] C. Lecaplain, C. Javerzac-Galy, M.L. Gorodetsky, T.J. Kippenberg, Mid-infrared ultra-high-Q resonators based on fluoride crystalline materials, Nat. Commun. 7 (2016) 13383.
[72] Y. Dumeige, S. Trebaol, L. Ghişa, T.K.N. Nguyen, H. Tavernier, P. Féron, Determination of coupling regime of high-Q resonators and optical gain of highly selective amplifiers, JOSA B 25 (2008) 2073–2080.
[73] Y.K. Chembo, D.V. Strekalov, N. Yu, Spectrum and dynamics of optical frequency combs generated with whispering gallery mode resonators, Phys. Rev. Lett. 104 (2010) 103902.
[74] A. Coillet, I. Balakireva, R. Henriet, K. Saleh, L. Larger, J. Dudley, C. Menyuk, Y.K. Chembo, Azimuthal turing patterns, bright and dark cavity solitons in Kerr combs generated with whispering gallery mode resonators, IEEE Phot. J. 5 (2013) 6100409.
[75] G. Lin, Y.K. Chembo, On the dispersion management of fluorite whispering-gallery mode resonators for Kerr optical frequency comb generation in the telecom and mid-infrared range, Optic Express 23 (2015) 1594–1604.
[76] K. Saleh, Y.K. Chembo, Optimization of close-in phase noise for microwaves generated with Kerr combs using brillouin-assisted pump depletion, IEEE Phot. J. 8 (2016) 5501807.
[77] K. Saleh, Y.K. Chembo, On the phase noise performance of microwave and millimeter-wave signals generated with versatile Kerr optical frequency combs, Optic Express 24 (2016) 25043–25056.
[78] J. Pfeifle, A. Coillet, R. Henriet, K. Saleh, P. Schindler, C. Weimann, W. Freude, I.V. Balakireva, L. Larger, C. Koos, Y.K. Chembo, Optimally coherent Kerr combs generated with crystalline whispering gallery mode resonators for ultrahigh capacity fiber communications, Phys. Rev. Lett. 114 (2015) 093902.
[79] A. Coillet, Y.K. Chembo, Routes to spatiotemporal chaos in Kerr optical frequency combs, Chaos 24 (2014) 013313.
[80] A. Coillet, Y.K. Chembo, On the robustness of phase-locking in Kerr optical frequency combs, Opt. Lett. 39 (2014) 1529–1532.
[81] G. Lin, Y.K. Chembo, Phase-locking transition in Raman combs generated with whispering gallery mode resonators, Opt. Lett. 41 (2016) 3718–3721.
[82] S. Diallo, Y.K. Chembo, Optimization of primary Kerr optical frequency combs for tunable microwave generation, Opt. Lett. 42 (2016) 3522–3525.
[83] G. Lin, B. Qian, F. Orucević, Y. Candela, J.-B. Jager, Z. Cai, V. Lefèvre-Seguin, J. Hare, Excitation mapping of whispering gallery modes in silica microcavities, Opt. Lett. 35 (2010) 583–585.
[84] X. Jin, Y. Dong, K. Wang, Selective excitation of axial modes in a high-Q microcylindrical resonator for controlled and robust coupling, Appl. Opt. 54 (2015) 8100–8107.
[85] T. Carmon, L. Yang, K.J. Vahala, Dynamical thermal behavior and thermal selfstability of microcavities, Optic Express 12 (2004) 4742–4750.
[86] G. Lin, Y. Candela, O. Tillement, Z. Cai, V. Lefèvre-Seguin, J. Hare, Thermal bistability-based method for real-time optimization of ultralow-threshold whispering gallery mode microlasers, Opt. Lett. 37 (2012) 5193–5195.
[87] S. Diallo, G. Lin, Y.K. Chembo, Giant thermo-optical relaxation oscillations in millimeter-size whispering gallery mode disk resonators, Opt. Lett. 40 (2015) 3834–3837.
[88] Y.K. Chembo, L. Baumgartel, N. Yu, Neutral mounting of ultrahigh Q whispering gallery mode disc-resonators for metrological applications, IEEE Photonics J 9 (2017) 6800308.
[89] W. Koechner, Solid-State Laser Engineering, Springer, 2006.
[90] M. Lax, Classical noise. v. noise in self-sustained oscillators, Phys. Rev. 160 (1967) 290.
[91] T.J. Kane, R.L. Byer, Monolithic, unidirectional single-mode Nd:YAG ring laser, Opt. Lett. 10 (1985) 65–67.
[92] G. Lin, Y. Cao, Z. Lu, Y.K. Chembo, Spontaneous generation of orbital angular momentum crystals using a monolithic Nd:YAG nonplanar ring laser, Opt. Lett. 44 (2019) 203–206.
[93] A.C. Nilsson, E.K. Gustafson, R.L. Byer, Eigenpolarization theory of monolithic nonplanar ring oscillators, IEEE J. Quantum Electron. 25 (1989) 767–790.
[94] P. Kwee, C. Bogan, K. Danzmann, M. Frede, H. Kim, P. King, J. Pold, O. Puncken, R.L. Savage, F. Seifert, et al., Stabilized high-power laser system for the gravitational wave detector advanced LIGO, Optic Express 20 (2012) 10617–10634.
[95] LISA-Collaboration, The lisa pathfinder mission, J. Phys. Conf. Ser. 610 (2015) 012005.
[96] P. Burdack, T. Fox, M. Bode, I. Freitag, 1 W of stable single-frequency output at 1.03 μm from a novel, monolithic, non-planar Yb:YAG ring laser operating at room temperature, Optic Express 14 (2006) 4363–4367.
[97] B.-Q. Yao, X.-M. Duan, D. Fang, Y.-J. Zhang, L. Ke, Y.-L. Ju, Y. zhu Wang, G.-J. Zhao, 7.3 W of single-frequency output power at 2.09 μm from an Ho:YAG monolithic nonplanar ring laser, Opt. Lett. 33 (2008) 2161–2163.
[98] C. Gao, M. Gao, Y. Zhang, Z. Lin, L. Zhu, Stable single-frequency output at 2.01 μm from a diode-pumped monolithic double diffusion-bonded Tm:YAG nonplanar ring oscillator at room temperature, Opt. Lett. 34 (2009) 3029–3031.
[99] D.-W. Chen, P.M. Belden, T.S. Rose, S.M. Beck, Narrowband Er:YAG nonplanar ring oscillator at 1645 nm, Opt. Lett. 36 (2011) 1197–1199.
[100] C. Gao, L. Zhu, R. Wang, M. Gao, Y. Zheng, L. Wang, 6.1 W single frequency laser output at 1645 nm from a resonantly pumped Er:YAG nonplanar ring oscillator, Opt. Lett. 37 (2012) 1859–1861.
[101] R. Wang, C. Gao, Y. Zheng, M. Gao, Q. Ye, A resonantly pumped 1645 nm Er:YAG nonplanar ring oscillator with 10.5 W single frequency output, IEEE Photonics Technol. Lett. 25 (2013) 955–957.
[102] L. Wang, C. Gao, M. Gao, Y. Li, Resonantly pumped monolithic nonplanar Ho:YAG ring laser with high-power single-frequency laser output at 2122 nm, Optic Express 21 (2013) 9541–9546.
[103] Y. Zheng, C. Gao, R. Wang, M. Gao, Q. Ye, Single frequency 1645 nm Er:YAG nonplanar ring oscillator resonantly pumped by a 1470 nm laser diode, Opt. Lett. 38 (2013) 784–786.
[104] W. Deng, T. Yang, J. Cao, E. Zang, L. Li, L. Chen, Z. Fang, High-efficiency 1064 nm nonplanar ring oscillator Nd:YAG laser with diode pumping at 885 nm, Opt. Lett. 43 (2018) 1562–1565.
[105] G. Lin, Y. Cao, R. Ji, C. Hou, Z. Lu, Direct generation of a narrow-linewidth Laguerre-Gaussian vortex laser in a monolithic nonplanar oscillator, Opt. Lett. 43 (2018) 4164–4167.
[106] A.M. Yao, M.J. Padgett, Orbital angular momentum: origins, behavior and applications, Adv. Opt. Photon 3 (2011) 161–204.
[107] A.E. Willner, H. Huang, Y. Yan, Y. Ren, N. Ahmed, G. Xie, C. Bao, L. Li, Y. Cao, Z. Zhao, J. Wang, M.P.J. Lavery, M. Tur, S. Ramachandran, A.F. Molisch, N. Ashrafi, S. Ashrafi, Optical communications using orbital angular momentum beams, Adv. Opt. Photon 7 (2015) 66–106.
[108] N. Schine, A. Ryou, A. Gromov, A. Sommer, J. Simon, Synthetic landau levels for photons, Nature 534 (2016) 671.
[109] S.J. Herr, K. Buse, I. Breunig, LED-pumped whispering-gallery laser, Photon. Res. 5 (2017) B34–B38.
[110] Y. Wang, V.D. Ta, K.S. Leck, B.H.I. Tan, Z. Wang, T. He, C.-D. Ohl, H.V. Demir, H. Sun, Robust whispering-gallery-mode microbubble lasers from colloidal quantum dots, Nano Lett. 17 (2017) 2640–2646.
[111] M. Humar, S.H. Yun, Whispering-gallery-mode emission from biological luminescent protein microcavity assemblies, Optica 4 (2017) 222–228.
[112] K. Wang, S. Sun, C. Zhang, W. Sun, Z. Gu, S. Xiao, Q. Song, Whispering-gallery-mode based CH3NH3PbBr3 perovskite microrod lasers with high quality factors, Mater. Chem. Front. 1 (2017) 477–481.
[113] V. Reboud, A. Gassenq, N. Pauc, J. Aubin, L. Milord, Q. Thai, M. Bertrand, K. Guilloy, D. Rouchon, J. Rothman, et al., Optically pumped gesn micro-disks with 16% Sn lasing at 3.1 μ m up to 180 K, Appl. Phys. Lett. 111 (2017) 092101.
[114] L. Wan, H. Chandrahalim, J. Zhou, Z. Li, C. Chen, S. Cho, H. Zhang, T. Mei, H. Tian, Y. Oki, et al., Demonstration of versatile whispering-gallery micro-lasers for remote refractive index sensing, Optic Express 26 (2018) 5800–5809.
[115] G. Zhu, J. Li, J. Li, J. Guo, J. Dai, C. Xu, Y. Wang, Single-mode ultraviolet whispering gallery mode lasing from a floating GaN microdisk, Opt. Lett. 43 (2018) 647–650.
[116] S. Han, W. Zhang, B. Qiu, H. Dong, W. Chen, M. Chu, Y. Liu, X. Yang, F. Hu, Y.S. Zhao, Controlled assembly of organic composite microdisk/microwire heterostructures for output coupling of dual-color lasers, Adv. Opt. Mater. 6 (2018) 1701077.
[117] T. Siegle, J. Kellerer, M. Bonenberger, S. Krämmer, C. Klusmann, M. Müller, H. Kalt, Comparison of various excitation and detection schemes for dye-doped polymeric whispering gallery mode micro-lasers, Optic Express 26 (2018) 3579–3593.
[118] S.-J. Tang, Z. Liu, Y.-J. Qian, K. Shi, Y. Sun, C. Wu, Q. Gong, Y.-F. Xiao, A tunable optofluidic microlaser in a photostable conjugated polymer, Adv. Mater. (2018) 1804556.
[119] L. Jin, Y. Wu, Y. Wang, S. Liu, Y. Zhang, Z. Li, X. Chen, W. Zhang, S. Xiao, Q. Song, Mass-manufactural lanthanide-based ultraviolet B microlasers, Adv. Mater. (2018) 1807079.
[120] S. Wang, Y. Liu, G. Li, J. Zhang, N. Zhang, S. Xiao, Q. Song, Lead halide perovskite based microdisk lasers for on-chip integrated photonic circuits, Adv. Opt. Mater. 6 (2018) 1701266.
[121] M. Feng, J. He, Q. Sun, H. Gao, Z. Li, Y. Zhou, J. Liu, S. Zhang, D. Li, L. Zhang, X. Sun, D. Li, H. Wang, M. Ikeda, R. Wang, H. Yang, Room-temperature electrically pumped InGaN-based microdisk laser grown on Si, Optic Express 26 (2018) 5043–5051.
[122] D. Ristić, A. Chiappini, M. Mazzola, P. Féron, H. Gebavi, M. Ivanda, M. Ferrari, Lasing and mode selection in erbium doped $70SiO_2$-$30HfO_2$ coated microspheres, Opt. Mater. 87 (2018) 98–101.
[123] P. Guo, M.K. Hossain, X. Shen, H. Sun, W. Yang, C. Liu, C.Y. Ho, C.K. Kwok, S.-W. Tsang, Y. Luo, et al., Room-temperature red–green–blue whispering-gallery mode lasing and white-light emission from cesium lead halide perovskite ($CsPbX_3$, X= Cl, Br, I) microstructures, Adv. Opt. Mater. 6 (2018) 1700993.
[124] R. Galiev, N. Pavlov, N. Kondratiev, S. Koptyaev, V. Lobanov, A. Voloshin, A. Gorodnitskiy, M. Gorodetsky, Spectrum collapse, narrow linewidth, and Bogatov effect in diode lasers locked to high-Q optical microresonators, Optic Express 26 (2018) 30509–30522.
[125] X.-F. Liu, T.-J. Wang, C. Wang, Optothermal control of gains in erbium-doped whispering-gallery microresonators, Opt. Lett. 43 (2018) 326–329.
[126] R. Ma, S. Yuan, S. Zhu, L. Shi, X. Zhang, Tunable sub-kHz single-mode fiber laser based on a hybrid microbottle resonator, Opt. Lett. 43 (2018) 5315–5318.
[127] C. Xu, F. Qin, Q. Zhu, J. Lu, Y. Wang, J. Li, Y. Lin, Q. Cui, Z. Shi, A.G. Manohari, Plasmon-enhanced ZnO whispering-gallery mode lasing, Nano Research 11 (2018) 3050–3064.
[128] M. Díaz, L.E. Scholz, J. Marrero-Alonso, A. Boto, R. Marín, F. Lobo, D. Hernández,

A. Amesty, A. Estévez-Braun, D. Quinto-Alemany, R. Puertas-Avedaño, F. Lahoz, Opto-chemical and laser properties of FLTX1, a novel fluorescent tamoxifen derivative, and its potential applications in breast cancer photodynamic chemotherapy, Opt. Mater. 84 (2018) 442–446.
[129] L. de Sousa-Vieira, S. Ríos, I. Martín, L. García-Rodríguez, V. Sigaev, V. Savinkov, G.Y. Shakhgildyan, Whispering gallery modes in a holmium doped glass microsphere: temperature sensor in the second biological window, Opt. Mater. 83 (2018) 207–211.
[130] A. Petermann, T. Hildebrandt, U. Morgner, B. Roth, M. Meinhardt-Wollweber, Polymer based whispering gallery mode humidity sensor, Sensors 18 (2018) 2383.
[131] J.R. Lopez, E. Treasurer, K.M. Snyder, D. Keng, S. Arnold, Whispering gallery mode coulometry of the nanoparticle-microcavity interaction in aqueous solution, Appl. Phys. Lett. 112 (2018) 051109.
[132] T. Kumagai, N. Hirota, K. Sato, K. Namiki, H. Maki, T. Tanabe, Saturable absorption by carbon nanotubes on silica microtoroids, J. Appl. Phys. 123 (2018) 233104.
[133] I. Kalyan, C. Krishnamurthy, Morphology dependent resonance modes in highly porous TiO_2 microspheres, J. Appl. Phys. 124 (2018) 133102.
[134] A. Fernandez-Bravo, K. Yao, E.S. Barnard, N.J. Borys, E.S. Levy, B. Tian, C.A. Tajon, L. Moretti, M.V. Altoe, S. Aloni, et al., Continuous-wave upconverting nanoparticle microlasers, Nat. Nanotechnol. (2018) 1.
[135] S. Zhu, L. Shi, B. Xiao, X. Zhang, X. Fan, All-optical tunable microlaser based on an ultrahigh-q erbium-doped hybrid microbottle cavity, ACS Photonics 5 (9) (2018) 3794–3800.
[136] X.-F. Liu, F. Lei, T.-J. Wang, G.-L. Long, C. Wang, Gain lifetime characterization through time-resolved stimulated emission in a whispering-gallery mode microresonator, Nanophotonics 8 (1) (2018) 127–134.
[137] L. Yang, K.J. Vahala, Gain functionalization of silica microresonators, Opt. Lett. 28 (2003) 592.
[138] Ultra-low Threshold Lasing in Silica Whispering-Gallery-Mode Microcavities with Nd^{3+}:Gd_2O_3 Nanocrystals, Vol. vol. 7716.
[139] C.G.B. Garrett, W. Kaiser, W.L. Bond, Stimulated emission into optical whispering modes of spheres, Phys. Rev. 124 (1961) 1807–1809.
[140] T. Le, S.J. Schowalter, W. Rellergert, J. Jeet, G. Lin, N. Yu, E.R. Hudson, Low-threshold ultraviolet solid-state laser based on a Ce^{3+}:$LiCaAlF_6$ crystal resonator, Opt. Lett. 37 (2012) 4961–4963.
[141] V. Sandoghdar, F. Treussart, J. Hare, V. Lefèvre-Seguin, J.M. Raimond, S. Haroche, Very low threshold whispering-gallery-mode microsphere laser, Phys. Rev. A 54 (1996) R1777–R1780.
[142] J.L. Dominguez-Juarez, G. Kozyreff, J. Martorell, Whispering gallery microresonators for second harmonic light generation from a low number of small molecules, Nat. Commun. 2 (2011) 254.
[143] X. Zhang, Q.-T. Cao, Z. Wang, Y.-x. Liu, C.-W. Qiu, L. Yang, Q. Gong, Y.-F. Xiao, Symmetry-breaking-induced nonlinear optics at a microcavity surface, Nat. Photon. 13 (2019) 21.
[144] R.W. Boyd, Nonlinear Optics, second ed., Academic, 2003.
[145] G.P. Agrawal, Nonlinear Fiber Optics, fourth ed., Academic, 2007.
[146] G. Lin, J.U. Fürst, D.V. Strekalov, N. Yu, Wide-range cyclic phase matching and second harmonic generation in whispering gallery resonators, Appl. Phys. Lett. 103 (2013) 181107.
[147] G. Lin, N. Yu, Continuous tuning of double resonance-enhanced second harmonic generation in a dispersive dielectric resonator, Optic Express 22 (2014) 557–562.
[148] D. Gerstenberger, G. Tye, R. Wallace, Efficient second-harmonic conversion of cw single-frequency Nd: YAG laser light by frequency locking to a monolithic ring frequency doubler, Opt. Lett. 16 (1991) 992–994.
[149] D. Gerstenberger, R.W. Wallace, Continuous-wave operation of a doubly resonant lithium niobate optical parametric oscillator system tunable from 966 to 1185 nm, J. Opt. Soc. Am. B 10 (1993) 1681–1683.
[150] K. Fiedler, S. Schiller, R. Paschotta, P. Kürz, J. Mlynek, Highly efficient frequency doubling with a doubly resonant monolithic total-internal-reflection ring resonator, Opt. Lett. 18 (1993) 1786–1788.
[151] S. Schiller, R.L. Byer, Quadruply resonant optical parametric oscillation in a monolithic total-internal-reflection resonator, J. Opt. Soc. Am. B 10 (1993) 1696–1707.
[152] J.D. Vance, C.-Y. She, H. Moosmüller, Continuous-wave, all-solid-state, single-frequency 400-mW source at 589 nm based on doubly resonant sum-frequency mixing in a monolithic lithium niobate resonator, Appl. Opt. 37 (1998) 4891–4896.
[153] A. Brieussel, Y. Shen, G. Campbell, G. Guccione, J. Janousek, B. Hage, B. Buchler, N. Treps, C. Fabre, F. Fang, et al., Squeezed light from a diamond-turned monolithic cavity, Optic Express 24 (2016) 4042–4056.
[154] V.S. Ilchenko, A. a. Savchenkov, A.B. Matsko, L. Maleki, Nonlinear optics and crystalline whispering gallery mode cavities, Phys. Rev. Lett. 92 (2004) 043903.
[155] J.U. Fürst, D.V. Strekalov, D. Elser, M. Lassen, U.L. Andersen, C. Marquardt, G. Leuchs, Naturally phase-matched second-harmonic generation in a whispering-gallery-mode resonator, Phys. Rev. Lett. 104 (2010) 153901.
[156] J. Lin, Y. Xu, J. Ni, M. Wang, Z. Fang, L. Qiao, W. Fang, Y. Cheng, Phase-matched second-harmonic generation in an on-chip linbo3 microresonator, Phys. Rev. Appl 6 (2016) 014002.
[157] L.S. Trainor, F. Sedlmeir, C. Peuntinger, H.G. Schwefel, Selective coupling enhances harmonic generation of whispering-gallery modes, Phys. Rev. Appl 9 (2018) 024007.
[158] J. Lin, N. Yao, Z. Hao, J. Zhang, W. Mao, M. Wang, W. Chu, R. Wu, Z. Fang, L. Qiao, et al., Broadband quasi-phase-matched harmonic generation in an on-chip monocrystalline lithium niobate microdisk resonator, Phys. Rev. Lett. 122 (17) (2019) 173903.
[159] K. Sasagawa, M. Tsuchiya, Highly efficient third harmonic generation in a periodically poled MgO:LiNbO3 disk resonator, APEX 2 (2009) 122401.
[160] J.U. Fürst, D.V. Strekalov, D. Elser, A. Aiello, U.L. Andersen, C. Marquardt, G. Leuchs, Low-threshold optical parametric oscillations in a whispering gallery mode resonator, Phys. Rev. Lett. 105 (2010) 263904.
[161] J. Moore, M. Tomes, T. Carmon, M. Jarrahi, Continuous-wave ultraviolet emission through fourth-harmonic generation in a whispering-gallery resonator, Optic Express 19 (2011) 24139–24146.
[162] T. Beckmann, H. Linnenbank, H. Steigerwald, B. Sturman, D. Haertle, K. Buse, I. Breunig, Highly tunable low-threshold optical parametric oscillation in radially poled whispering gallery resonators, Phys. Rev. Lett. 106 (2011) 143903.
[163] C.S. Werner, T. Beckmann, K. Buse, I. Breunig, Blue-pumped whispering gallery optical parametric oscillator, Opt. Lett. 37 (2012) 4224–4226.
[164] G. Schunk, U. Vogl, D.V. Strekalov, M. Förtsch, F. Sedlmeir, H.G.L. Schwefel, M. Göbelt, S. Christiansen, G. Leuchs, C. Marquardt, Interfacing transitions of different alkali atoms and telecom bands using one narrowband photon pair source, Optica 2 (2015) 773.
[165] C.S. Werner, K. Buse, I. Breunig, Continuous-wave whispering-gallery optical parametric oscillator for high-resolution spectroscopy, Opt. Lett. 40 (2015) 772–775.
[166] Q. Mo, S. Li, Y. Liu, X. Jiang, G. Zhao, Z. Xie, X. Lv, S. Zhu, Widely tunable optical parametric oscillator in periodically poled congruently grown lithium tantalite whispering gallery mode resonators, Chin. Optic Lett. 14 (2016) 091902.
[167] D.V. Strekalov, A.S. Kowligy, Y.-P. Huang, P. Kumar, Optical sum-frequency generation in a whispering-gallery-mode resonator, New J. Phys. 16 (2014) 053025.
[168] J. Lin, Y. Xu, Z. Fang, M. Wang, J. Song, N. Wang, L. Qiao, W. Fang, Y. Cheng, Fabrication of high-Q lithium niobate microresonators using femtosecond laser micromachining, Sci. Rep. 5 (2015) 8072.
[169] S.-K. Meisenheimer, J.U. Fürst, C. Werner, T. Beckmann, K. Buse, I. Breunig, Broadband infrared spectroscopy using optical parametric oscillation in a radially-poled whispering gallery resonator, Optic Express 23 (2015) 24042.
[170] R. Luo, H. Jiang, S. Rogers, H. Liang, Y. He, Q. Lin, On-chip second-harmonic generation and broadband parametric down-conversion in a lithium niobate microresonator, Optic Express 25 (2017) 24531–24539.
[171] S. Liu, Y. Zheng, X. Chen, Cascading second-order nonlinear processes in a lithium niobate-on-insulator microdisk, Opt. Lett. 42 (2017) 3626–3629.
[172] R. Wu, J. Zhang, N. Yao, W. Fang, L. Qiao, Z. Chai, J. Lin, Y. Cheng, Lithium niobate micro-disk resonators of quality factors above 10^7, Opt. Lett. 43 (2018) 4116–4119.
[173] J. Lin, Y. Ni, Z. Hao, J. Zhang, W. Mao, M. Wang, W. Chu, R. Wu, Z. Fang, L. Qiao, et al., Highly-efficient Second and Third Harmonic Generation in a Monocrystalline Lithium Niobate Microresonator, (2018) arXiv preprint arXiv:1809.04523.
[174] Z. Hao, L. Zhang, A. Gao, W. Mao, X. Lyu, X. Gao, F. Bo, F. Gao, G. Zhang, J. Xu, Periodically poled lithium niobate whispering gallery mode microcavities on a chip, Sci. China Phys. Mech. Astron. 61 (2018) 114211.
[175] Y. Pan, G. Lin, S. Diallo, X. Zhang, Y.K. Chembo, Design of X-cut and Z-cut lithium niobate whispering-gallery-mode disk-resonators with high quality factors, IEEE Photon. J. 9 (2017) 2700608.
[176] G. Lin, J. Fürst, D.V. Strekalov, I.S. Grudinin, N. Yu, High-Q UV whispering gallery mode resonators made of angle-cut BBO crystals, Optic Express 20 (2012) 21372.
[177] P.S. Kuo, J. Bravo-Abad, G.S. Solomon, Second-harmonic generation using -quasi-phasematching in a GaAs whispering-gallery-mode microcavity, Nat. Commun. 5 (2014) 3109.
[178] S. Mariani, A. Andronico, A. Lemaître, I. Favero, S. Ducci, G. Leo, Second-harmonic generation in AlGaAs microdisks in the telecom range, Opt. Lett. 39 (2014) 3062.
[179] J.U. Fürst, K. Buse, I. Breunig, P. Becker, J. Liebertz, L. Bohatý, Second-harmonic generation of light at 245 nm in a lithium tetraborate whispering gallery resonator, Opt. Lett. 40 (2015) 1932–1935.
[180] N. Vukovic, N. Healy, J.R. Sparks, J.V. Badding, P. Horak, A.C. Peacock, Tunable continuous wave emission via phase-matched second harmonic generation in a ZnSe microcylindrical resonator, Sci. Rep. 5 (2015) 11798.
[181] I. Roland, M. Gromovyi, Y. Zeng, M. El Kurdi, S. Sauvage, C. Brimont, T. Guillet, B. Gayral, F. Semond, J.-Y. Duboz, et al., Phase-matched second harmonic generation with on-chip GaN-on-Si microdisks, Sci. Rep. 6 (2016) 34191.
[182] P. Guillemé, M. Vallet, J. Stodolna, A. Ponchet, C. Cornet, A. Létoublon, P. Féron, O. Durand, Y. Léger, Y. Dumeige, Antiphase domain tailoring for combination of modal and 4 -quasi-phase matching in gallium phosphide microdisks, Optic Express 24 (2016) 14608.
[183] S.-K. Meisenheimer, J.U. Fürst, K. Buse, I. Breunig, Continuous-wave optical parametric oscillation tunable up to an 8 μm wavelength, Optica 4 (2017) 189–192.
[184] Y. Jia, K. Hanka, K.T. Zawilski, P.G. Schunemann, K. Buse, I. Breunig, Continuous-wave whispering-gallery optical parametric oscillator based on $CdSiP_2$, Optic Express 26 (2018) 10833–10841.
[185] X. Lin, Y. Liu, K. Wang, C. Wei, W. Zhang, Y. Yan, Y.J. Li, J. Yao, Y.S. Zhao, Two-dimensional pyramid-like WS_2 layered structures for highly efficient edge second-harmonic generation, ACS Nano 12 (2018) 689–696 pMID: 29294288.
[186] Q. Ai, L. Gui, D. Paone, B. Metzger, M. Mayer, K. Weber, A. Fery, H. Giessen, Ultranarrow second-harmonic resonances in hybrid plasmon-fiber cavities, Nano Lett. 18 (2018) 5576–5582 pMID: 30075631.
[187] S.M. Spillane, T.J. Kippenberg, K.J. Vahala, Ultralow-threshold Raman laser using a spherical dielectric microcavity, Nature 415 (2002) 621–623.
[188] T.J. Kippenberg, S.M. Spillane, K.J. Vahala, Kerr-nonlinearity optical parametric oscillation in an ultrahigh-Q toroid microcavity, Phys. Rev. Lett. 93 (2004) 083904.
[189] T.J. Kippenberg, S.M. Spillane, D.K. Armani, K.J. Vahala, Ultralow-threshold microcavity Raman laser on a microelectronic chip, Opt. Lett. 29 (2004) 1224–1226.
[190] L. Yang, T. Carmon, B. Min, S.M. Spillane, K.J. Vahala, Erbium-doped and Raman microlasers on a silicon chip fabricated by the solgel process, Appl. Phys. Lett. 86 (2005) 091114.
[191] T. Carmon, K.J. Vahala, Visible continuous emission from a silica microphotonic

device by third-harmonic generation, Nat. Phys. 3 (2007) 430.
[192] P. DelHaye, A. Schliesser, O. Arcizet, T. Wilken, R. Holzwarth, T.J. Kippenberg, Optical frequency comb generation from a monolithic microresonator, Nature 450 (2007) 1214.
[193] X.-F. Jiang, Y.-F. Xiao, Q.-F. Yang, L. Shao, W.R. Clements, Q. Gong, Free-space coupled, ultralow-threshold Raman lasing from a silica microcavity, Appl. Phys. Lett. 103 (2013) 101102.
[194] D. Farnesi, F. Cosi, C. Trono, G.C. Righini, G.N. Conti, S. Soria, Stimulated anti-Stokes Raman scattering resonantly enhanced in silica microspheres, Opt. Lett. 39 (2014) 5993.
[195] B.-B. Li, W.R. Clements, X.-C. Yu, K. Shi, Q. Gong, Y.-F. Xiao, Single nanoparticle detection using split-mode microcavity Raman lasers, Proc. Natl. Acad. Sci. U.S.A. 111 (2014) 14657–14662.
[196] W.R. Clements, B.-B. Li, B.-Q. Shen, Y.-F. Xiao, Raman-lasing dynamics in split-mode microresonators, Phys. Rev. A 91 (2015) 013804.
[197] D. Farnesi, A. Barucci, G.C. Righini, G.N. Conti, S. Soria, Generation of hyper-parametric oscillations in silica microbubbles, Opt. Lett. 40 (2015) 4508–4511.
[198] Y. Ooka, Y. Yang, J. Ward, S.N. Chormaic, Raman lasing in a hollow, bottle-like microresonator, APEX 8 (2015) 092001.
[199] Q. Lu, S. Liu, X. Wu, L. Liu, L. Xu, Stimulated Brillouin laser and frequency comb generation in high-Q microbubble resonators, Opt. Lett. 41 (8) (2016) 1736–1739.
[200] M. Asano, Y. Takeuchi, S.K. Ozdemir, R. Ikuta, L. Yang, N. Imoto, T. Yamamoto, Stimulated brillouin scattering and Brillouin-coupled four-wave-mixing in a silica microbottle resonator, Optic Express 24 (2016) 12082–12092.
[201] Q. Lu, S. Liu, X. Wu, L. Liu, L. Xu, Stimulated Brillouin laser and frequency comb generation in high-Q microbubble resonators, Opt. Lett. 41 (2016) 1736–1739.
[202] Y. Yang, X. Jiang, S. Kasumie, G. Zhao, L. Xu, J.M. Ward, L. Yang, S.N. Chormaic, Four-wave mixing parametric oscillation and frequency comb generation at visible wavelengths in a silica microbubble resonator, Opt. Lett. 41 (2016) 5266–5269.
[203] S. Fujii, T. Kato, R. Suzuki, T. Tanabe, Third-harmonic blue light generation from kerr clustered combs and dispersive waves, Opt. Lett. 42 (2017) 2010–2013.
[204] Y. Chen, Z.-H. Zhou, C.-L. Zou, Z. Shen, G.-C. Guo, C.-H. Dong, Tunable Raman laser in a hollow bottle-like microresonator, Optic Express 25 (2017) 16879–16887.
[205] T. Kato, A. Hori, R. Suzuki, S. Fujii, T. Kobatake, T. Tanabe, Transverse mode interaction via stimulated Raman scattering comb in a silica microcavity, Optic Express 25 (2017) 857–866.
[206] X. Jiang, L. Shao, S.-X. Zhang, X. Yi, J. Wiersig, L. Wang, Q. Gong, M. Lončar, L. Yang, Y.-F. Xiao, Chaos-assisted broadband momentum transformation in optical microresonators, Science 358 (2017) 344–347.
[207] Y. Honda, W. Yoshiki, T. Tetsumoto, S. Fujii, K. Furusawa, N. Sekine, T. Tanabe, Brillouin lasing in coupled silica toroid microcavities, Appl. Phys. Lett. 112 (2018) 201105.
[208] R. Suzuki, A. Kubota, A. Hori, S. Fujii, T. Tanabe, Broadband gain induced Raman comb formation in a silica microresonator, J. Opt. Soc. Am. B 35 (2018) 933–938.
[209] S. Fujii, T. Kato, R. Suzuki, A. Hori, T. Tanabe, Transition between Kerr comb and stimulated Raman comb in a silica whispering gallery mode microcavity, J. Opt. Soc. Am. B 35 (2018) 100–106.
[210] C.-H. Dong, Z. Shen, C.-L. Zou, Y.-L. Zhang, W. Fu, G.-C. Guo, Brillouin-scattering-induced transparency and non-reciprocal light storage, Nat. Commun. 6 (2015) 6193.
[211] J. Kim, M.C. Kuzyk, K. Han, H. Wang, G. Bahl, Non-reciprocal Brillouin scattering induced transparency, Nat. Phys. 11 (2015) 275.
[212] J. Ma, L. Xiao, J. Gu, H. Li, X. Cheng, G. He, X. Jiang, M. Xiao, Visible kerr comb generation in a high-q silica microdisk resonator with a large wedge angle, Photon. Res. 7 (5) (2019) 573–578.
[213] S. Jiang, C. Guo, K. Che, Z. Luo, T. Du, H. Fu, H. Xu, Z. Cai, Visible Raman and brillouin lasers from a microresonator/zblan-fiber hybrid system, Photon. Res. 7 (5) (2019) 566–572.
[214] S.B. Papp, S.A. Diddams, Spectral and temporal characterization of a fused-quartz-microresonator optical frequency comb, Phys. Rev. A 84 (2011) 053833.
[215] A. Coillet, R. Henriet, K.P. Huy, M. Jacquot, L. Furfaro, I. Balakireva, L. Larger, Y.K. Chembo, Microwave photonics systems based on whispering-gallery-mode resonators, J. Vis. Exp. 78 (2013) e50423.
[216] I.S. Grudinin, L. Maleki, Ultralow-threshold Raman lasing with CaF_2 resonators, Opt. Lett. 32 (2007) 166–168.
[217] I.S. Grudinin, A.B. Matsko, L. Maleki, Brillouin lasing with a CaF_2 whispering gallery mode resonator, Phys. Rev. Lett. 102 (2009) 043902.
[218] H. Tavernier, P. Salzenstein, K. Volyanskiy, Y.K. Chembo, L. Larger, Magnesium fluoride whispering gallery mode disk-resonators for microwave photonics applications, IEEE Photonics Technol. Lett. 22 (22) (2010) 1629–1631.
[219] W. Liang, V.S. Ilchenko, A.A. Savchenkov, A.B. Matsko, D. Seidel, L. Maleki, Passively mode-locked Raman laser, Phys. Rev. Lett. 105 (2010) 143903.
[220] R. Henriet, A. Coillet, K. Saleh, L. Larger, Y.K. Chembo, Barium fluoride and lithium fluoride whispering-gallery-mode resonators for photonics applications, Opt. Eng. 53 (2014) 071821.
[221] G. Lin, S. Diallo, K. Saleh, R. Martinenghi, J.-C. Beugnot, T. Sylvestre, Y.K. Chembo, Cascaded Brillouin lasing in monolithic barium fluoride whispering gallery mode resonators, Appl. Phys. Lett. 105 (2014) 231103.
[222] G. Lin, K. Saleh, R. Henriet, S. Diallo, R. Martinenghi, A. Coillet, Y.K. Chembo, Wide-range tunability, thermal locking, and mode-crossing effects in Kerr optical frequency combs, Opt. Eng. 53 (2014) 122602.
[223] T. Herr, V. Brasch, J.D. Jost, C.Y. Wang, N.M. Kondratiev, M.L. Gorodetsky, T.J. Kippenberg, Temporal solitons in optical microresonators, Nat. Photon. 8 (2014) 145–152.
[224] W. Liang, A.A. Savchenkov, Z. Xie, J.F. McMillan, J. Burkhart, V.S. Ilchenko, C.W. Wong, A.B. Matsko, L. Maleki, Miniature multioctave light source based on a monolithic microcavity, Optica 2 (2015) 40–47.
[225] G. Lin, R. Martinenghi, S. Diallo, K. Saleh, A. Coillet, Y.K. Chembo, Spectro-temporal dynamics of Kerr combs with parametric seeding, Appl. Opt. 54 (2015) 2407–2412.
[226] S. Diallo, G. Lin, R. Martinenghi, L. Furfaro, M. Jacquot, Y.K. Chembo, Brillouin lasing in ultra-high-Q lithium fluoride disk resonators, IEEE Photonics Technol. Lett. 28 (2016) 955–958.
[227] G. Lin, S. Diallo, J.M. Dudley, Y.K. Chembo, Universal nonlinear scattering in ultra-high Q whispering gallery-mode resonators, Optic Express 24 (2016) 14880.
[228] G. Lin, Y.K. Chembo, Opto-acoustic phenomena in whispering gallery mode resonators, Int. J. Optomechatronics 10 (2016) 32–39.
[229] W. Liang, V.S. Ilchenko, A.A. Savchenkov, A.B. Matsko, D. Seidel, L. Maleki, Whispering-gallery-mode-resonator-based ultranarrow linewidth external-cavity semiconductor laser, Opt. Lett. 35 (2010) 2822.
[230] W. Liang, V. Ilchenko, D. Eliyahu, A. Savchenkov, A. Matsko, D. Seidel, L. Maleki, Ultralow noise miniature external cavity semiconductor laser, Nat. Commun. 6 (2015) 7371.
[231] Y.K. Chembo, I.S. Grudinin, N. Yu, Spatiotemporal dynamics of Kerr-Raman optical frequency combs, Phys. Rev. A 92 (2015) 043818.
[232] Z. Bai, H. Yuan, Z. Liu, P. Xu, Q. Gao, R.J. Williams, O. Kitzler, R.P. Mildren, Y. Wang, Z. Lu, Stimulated Brillouin scattering materials, experimental design and applications: a review, Opt. Mater. 75 (2018) 626–645.
[233] S. Diallo, J.-P. Aubry, Y.K. Chembo, Effect of crystalline family and orientation on stimulated brillouin scattering in whispering-gallery mode resonators, Optic Express 25 (2017) 29934–29945.
[234] Y.K. Chembo, N. Yu, On the generation of octave-spanning optical frequency combs using monolithic whispering gallery mode micro-resonators, Opt. Lett. 35 (2010) 2696–2698.
[235] Y.K. Chembo, N. Yu, A modal expansion approach to optical frequency combs generation with monolithic whispering gallery mode resonators, Phys. Rev. A 82 (2010) 033801.
[236] I.V. Balakireva, Y.K. Chembo, A taxonomy of optical dissipative structures in whispering-gallery mode resonators with Kerr nonlinearity, Phil. Trans. R. Soc. A 376 (2018) 20170381.
[237] A. Coillet, J. Dudley, G. Genty, L. Larger, Y.K. Chembo, Optical rogue waves in whispering-gallery mode resonators, Phys. Rev. A 89 (2014) 013835.
[238] Y.K. Chembo, C.R. Menyuk, Spatiotemporal Lugiato-Lefever formalism for Kerr-comb generation in whispering-gallery mode resonators, Phys. Rev. A 87 (2013) 053852.
[239] J.H.T. Mbé, C. Milian, Y.K. Chembo, Existence and switching behavior of bright and dark Kerr solitons in whispering-gallery mode resonators with zero group-velocity dispersion, Eur. Phys. J. D 71 (2017) 196.
[240] C. Godey, I.V. Balakireva, A. Coillet, Y.K. Chembo, Stability analysis of the spatiotemporal Lugiato-Lefever model for Kerr optical frequency combs in the anomalous and normal dispersion regimes, Phys. Rev. A 89 (2014) 063814.
[241] T. Graziosi, S. Mi, M. Kiss, N. Quack, Single crystal diamond micro-disk resonators by focused ion beam milling, APL Photonics 3 (2018) 126101.
[242] F. Vanier, M. Rochette, N. Godbout, Y.-A. Peter, Raman lasing in As_2S_3 high-Q whispering gallery mode resonators, Opt. Lett. 38 (2013) 4966–4969.
[243] F. Vanier, Y.-A. Peter, M. Rochette, Cascaded Raman lasing in packaged high quality As_2S_3 microspheres, Optic Express 22 (2014) 28731–28739.
[244] C. Guo, K. Che, P. Zhang, J. Wu, Y. Huang, H. Xu, Z. Cai, Low-threshold stimulated Brillouin scattering in high-Q whispering gallery mode tellurite microspheres, Optic Express 23 (25) (2015) 32261–32266.
[245] H. Choi, A.M. Armani, Raman-Kerr frequency combs in Zr-doped silica hybrid microresonators, Opt. Lett. 43 (12) (2018) 2949–2952.
[246] S.H. Huang, X. Jiang, B. Peng, C. Janisch, A. Cocking, Şahin Kaya Özdemir, Z. Liu, L. Yang, Surface-enhanced Raman scattering on dielectric microspheres with whispering gallery mode resonance, Photon. Res. 6 (5) (2018) 346–356.
[247] S. Soltani, V.M. Diep, R. Zeto, A.M. Armani, Stimulated anti-Stokes Raman emission generated by gold nanorod coated optical resonators, ACS Photonics 5 (9) (2018) 3550–3556.
[248] Y.K. Chembo, Quantum dynamics of Kerr optical frequency combs below and above threshold: spontaneous four-wave mixing, entanglement, and squeezed states of light, Phys. Rev. A 93 (2016) 033820.